Electrified Nutrient Recovery at Municipal Wastewater Facilities: Sampling, Screening and Multivariate Analyses

Sana Heydarian[1#], Lawrence Ajayi[1#], Asad Syed Abbas[2], Kody Wolfe[2], Rida Benhaddou[3], Jason P. Trembly[2,4,5], Damilola A. Daramola[1,2,5,6*]

[1]Department of Chemical Engineering, Northeastern University, Boston MA 02115

[2]Institute for Sustainable Energy and the Environment, Department of Chemical and Biomolecular Engineering, Ohio University, Athens OH 45701

[3]Department of Mathematics, Ohio University, Athens OH 45701

[4]Department of Mechanical Engineering, Ohio University, Athens OH 45701

[5]Department of Chemical and Biomolecular Engineering, Ohio University, Athens OH 45701

[6]Department of Chemistry and Chemical Biology, Northeastern University, Boston MA 02115

[#]These authors contributed equally

[*]Corresponding Author: o.daramola@northeastern.edu

https://doi.org/10.26434/chemrxiv-2024-gwpw5 **ORCID:** https://orcid.org/0000-0002-6737-415X Content not peer-reviewed by ChemRxiv. **License:** CC BY-NC-ND 4.0

Abstract

Municipal wastewater facilities can contain recycle streams with high nutrient content, that both increase the overall energy consumption in the facility and cause environmental pollution when not properly handled. Reducing the nutrient load of these streams through recovery is a promising solution that enhances the Food-Energy-Water nexus by producing sustainable fertilizer. In this study, the potential for nutrient recovery at municipal wastewater facilities was investigated through a 1-year sampling of nutrient, ionic, organic and heavy metal composition of three wastewater streams influent to or effluent from two types of digesters. Subsequently, electrochemical nutrient recovery was evaluated for these streams through multivariate screening of three groups of variables – operational, stream and design – and the effect of these variables on optimal nutrient recovery in the form of phosphorus. Results showed that Orthophosphate (Ortho-P) and ammonia concentrations do not show significant correlation in any tested streams. On the other hand, major ions exhibited interdependence with Ortho-P concentration, while the stream pH was found to correlate with Ortho-P and Cl^- in the anaerobic digester effluent. Screening analyses identified 5 – anode type, cathodic potential, initial P concentration, initial NH_4^+ concentration and temperature – of the 11 variables evaluated were the variables that most significantly affected P recovery efficiency and specific energy consumed during this recovery. Finally, the optimum conditions for high phosphorus recovery and low energy consumption from the anaerobic digester effluent during a 2-hour experiment were a cathodic potential of -0.805 V vs $Ag/AgCl_{sat}$, an electrode area to electrolyte volume ratio of 0.145 1/cm, and a temperature of 41.3°C, with a solid product that was predominantly struvite. Overall, the demonstrated 95% P recovery efficiency and 0.03 kWh/kg P are characteristic of an emerging process that could be competitive at scale with state-of-the-art synthetic nutrient routes, if applied to the right stream.

https://doi.org/10.26434/chemrxiv-2024-gwpw5 **ORCID:** https://orcid.org/0000-0002-6737-415X Content not peer-reviewed by ChemRxiv. **License:** CC BY-NC-ND 4.0

Graphical Abstract

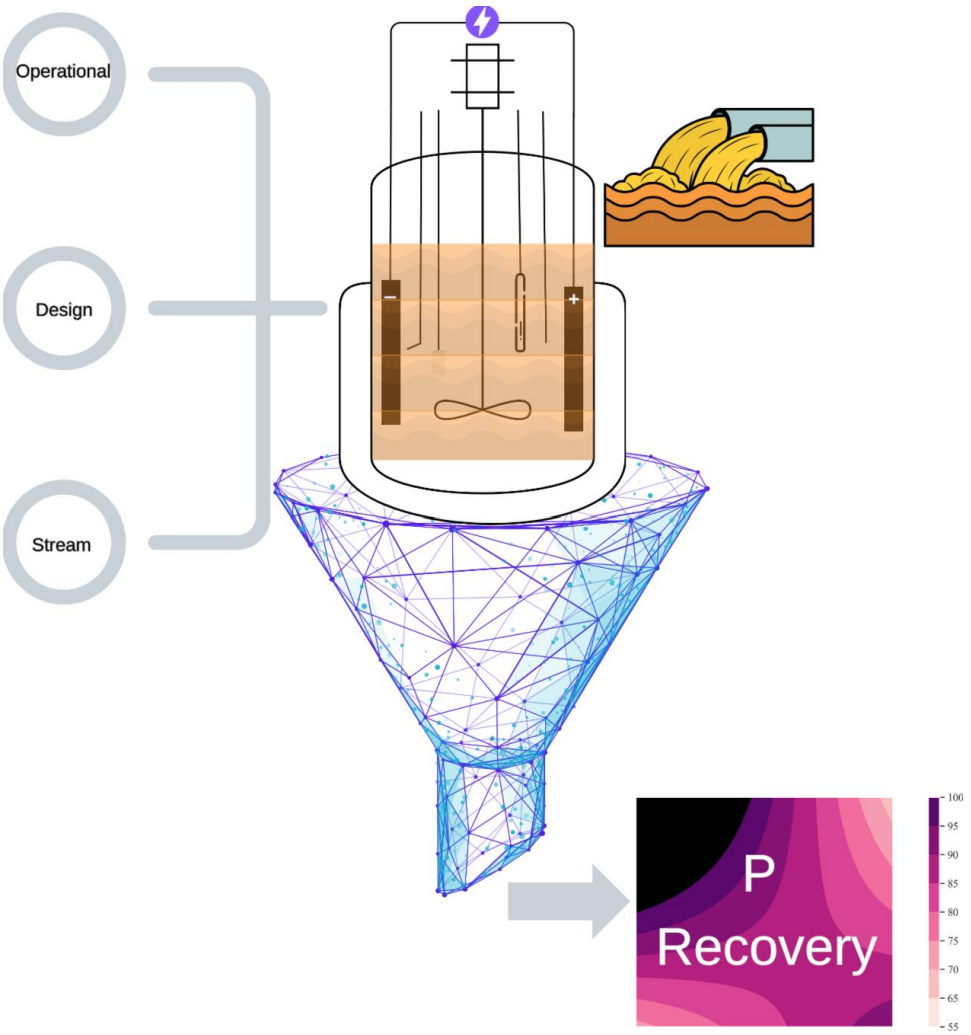

https://doi.org/10.26434/chemrxiv-2024-gwpw5 **ORCID:** https://orcid.org/0000-0002-6737-415X Content not peer-reviewed by ChemRxiv. **License:** CC BY-NC-ND 4.0

1 Introduction

About 35% of a municipality's total energy expenses can be attributed to the treatment systems of drinking water and wastewater [1,2]. High energy consumption in wastewater treatment plants (WWTPs) usually results from secondary treatment processes such as aeration which utilizes more than 50% of the total required energy [3,4]. This aeration is typically for supplying oxygen to microorganisms used for nitrification of ammonia (NH_3), even though water has limited capacity to dissolve oxygen (40 mg O_2/l vs 1450 mg CO_2/l at 25°C) resulting in increased costs for aeration [4,5]. Some treatment plants have integrated sludge digesters to both reduce the solid organic content handled at the facility, while also generating biogas that could be used to reduce the overall energy consumed by these facilities. However, this use of sludge digesters produces a supernatant with high Nitrogen (N) and Phosphorous (P) content [6]. This supernatant, which is recycled to the primary and secondary processes at WWTPs, increases the amount of coagulant required for reducing P load and energy consumption by aeration for reducing N load. Alternatively, the supernatant is used as a direct fertilizer on agricultural lands in some places, which can enhance nutrient leaching through the soil to water bodies [7,8]. This in turn, results in a surplus of nutrients in the water bodies and excessive algae growth, or eutrophication [7,9]. Therefore, due to energy costs and environmental regulations, it is important to decrease the nutrient load of the supernatant stream [8,10,11]. Additionally, this decreased load would further enhance the viability of converting wastewater treatment plants to water resource recovery facilities (WRRF) through the generation of water, re-usable energy and nutrients. In essence, this combination of wastewater treatment, energy recovery and nutrient availability is representative of a relevant challenge in the Food-Energy-Water nexus and the United Nations Sustainable Development Goals.

https://doi.org/10.26434/chemrxiv-2024-gwpw5 **ORCID:** https://orcid.org/0000-0002-6737-415X Content not peer-reviewed by ChemRxiv. **License:** CC BY-NC-ND 4.0

Different physiochemical processes have been used to decrease the nutrient load of the supernatant, such as NH_3 stripping, CO_2 stripping and membrane filtration [7,10,12–14]. Forward osmosis is also utilized to concentrate the supernatant to decrease its volume and extract less polluted water, but this method does not directly remove any nutrient from the stream, thus forward osmosis needs to be coupled with other operations [15]. Nutrients, specifically P, are currently removed in WWTPs through chemical precipitation, enhanced biological P removal, or a combination of both. Biological P removal involves either direct absorption of P by phosphorus-accumulating organisms (PAO), or improving the P storage capacity of the microorganism biomass [10,16]. Even though biological treatment offers lower operation costs as compared to physiochemical processes [7,17], this treatment results in excess sludge with high P concentrations that need additional treatment steps prior to environmental discharge [10,18]. On the other hand, chemical precipitation through the addition of metal ions such as iron (Fe) and aluminum (Al) coagulants removes P from wastewater [10,14,19,20], but limits P reusability as fertilizer due to the insoluble coagulant products [16,21]. Magnesium (Mg) and calcium (Ca)-driven chemical precipitation enable the recovery of P as a reusable product [10,21]. However, these chemical processes rely on pH adjustment through dosing with hydroxides, such as NaOH, and the costs associated with supplying the chemicals is a major drawback of these chemical P recovery technologies [22].

Alternatively, solution pH adjustment can be driven through electrochemistry, thereby facilitating nutrient recovery from municipal wastewater [23]. Water reduction (Equation 1) or oxygen reduction (Equation 2) at the cathode coupled with magnesium oxidation (Equation 3) at the anode can be used to drive the pH [24], or couple with water oxidation at the anode and dissolved magnesium salts in a reactor known as an electrolyzer.

https://doi.org/10.26434/chemrxiv-2024-gwpw5 **ORCID:** https://orcid.org/0000-0002-6737-415X Content not peer-reviewed by ChemRxiv. **License:** CC BY-NC-ND 4.0

Cathode:

$$2H_2O_{(l)} + 2e^- \rightarrow H_{2(g)} + 2OH^-_{(aq)} \quad (1)$$

$$O_{2(g)} + 2H_2O_{(l)} + 4e^- \rightarrow 4OH^-_{(aq)} \quad (2)$$

Anode (Sacrificial anode e.g., Magnesium)

$$Mg_{(s)} \rightarrow Mg^{2+}_{(aq)} + 2e^- \quad (3)$$

Anode (Non-sacrificial)

$$2H_2O_{(l)} \rightarrow O_{2(g)} + 4H^+_{(aq)} + 4e^- \quad (4)$$

This Electrified Nutrient Recovery (ENR) reduces or eliminates chemical addition by using electricity. Furthermore, ENR creates an additional driving force for ion migration via the potential gradient between the electrodes, thereby, enhancing the transport conditions for nutrient recovery[20]. ENR has been studied using different reactor configurations and wastewater streams. Lei *et al.*, while performing water reduction to drive pH, investigated the effect of applied current on P recovery from cheese wastewater and reported a recovery of 90% and energy consumption of 64.7 kWh/kg of P [25]. Belarbi *et al.* simulated animal waste and evaluated the effect of temperature, cathodic potential and turbulence on electrochemical P recovery via oxygen reduction, achieving a maximum recovery of 80% at 0.5 kWh/kg of P [20]. A sacrificial Mg anode was implemented by Kékedy-Nagy to study the effect of water chemistry on P recovery from poultry and municipal wastewater, obtaining a recovery range of 44.6 - 93% at 756-1181 kWh/kg of P [23]. Although these results established the prospect of ENR, integrating this technology in municipal WWTPs and future WRRFs requires investigating several factors that affect the efficiency of the system; factors not previously considered in the literature. These

https://doi.org/10.26434/chemrxiv-2024-gwpw5 **ORCID:** https://orcid.org/0000-0002-6737-415X Content not peer-reviewed by ChemRxiv. **License:** CC BY-NC-ND 4.0

factors include composition of the treated streams, the design and operation of the electrified process and how these factors significantly influence the type of recovered products and the energy consumed during this recovery process. This combination of analyses could provide an enhanced connectivity between the composition of the different wastewaters and the applied recovery process and provide a foundation for competing with state-of-the-art synthetic techniques that deliver the same nutrients at an industrial level.

In this study, we show the variability in the nutrient, ionic and heavy metal composition of post-digester streams based on samples collected over a one-year period and evaluate any time dependence of and correlation between the components assessed. This sampling assessment is key for identifying streams with potential value for nutrient recovery and may also provide additional descriptors for stream compositions based on correlated components. A recent review has quantified the general composition of different post-digester waste streams at various facilities in Europe [6]. However, prior to this review, this compositional information for recycle streams – typically called side streams – was unavailable in literature and the data in the review does not describe any time series effect. Next, we conducted a multivariate screening analysis of eleven variables associated with the stream chemistry, electrolyzer design and electrolyzer operation to characterize the factors that have the most significant impact on well-defined engineering figures of merit. This screening assessment could be indicative of the controls available for efficient deployment of this emerging approach, especially considering the variability in WWTP operations. Finally, we propose variables needed for optimal nutrient recovery by the electrolyzer using water from one of the sampled streams. Overall, this study represents a holistic and realistic investigation into integrating electrochemical nutrient recovery with a municipal wastewater treatment (and future recovery) facility and demonstrates the key

https://doi.org/10.26434/chemrxiv-2024-gwpw5 **ORCID:** https://orcid.org/0000-0002-6737-415X Content not peer-reviewed by ChemRxiv. **License:** CC BY-NC-ND 4.0

driving forces that may enable a circular nutrient recovery competitive with current state-of-the-art and synthetic routes.

2 Methodology

2.1 Wastewater Sampling and Characterization

Wastewater was collected approximately semi-monthly for one year (November 2021 to October 2022) from two different WWTPs in Ohio, U.S.A.: the 100 million gallons per day (MGD) Southerly WWTP in Columbus and the 4 MGD WWTP in Athens. At the Southerly WWTP, a plant with an anaerobic digester as illustrated in Figure S1, samples were collected from streams that make up the centrate stream of the facility: liquid from the post-digester dewatering centrifuge and liquid from the pre-digester thickening centrifuge. At the Athens WWTP, a plant with an aerobic digester, samples were collected from a post-digester settling tank. The sampled wastewater was analyzed for physical characteristics, chemical properties and species composition by MASI Environmental Laboratories, Plain City, Ohio. The methods used for each test can be found in Table S1. The pH and conductivity of each sample was also measured on the field (i.e., at the point of collection) using an ultra-meter (Myron L company) to cross-validate with the result from MASI Lab.

2.2 Time Series Analyses

The year-long municipal wastewater sampling results were used to investigate time-dependent trends and correlations between species within the three sampled streams. To determine the stationarity of each data series, for each species and stream combination, a Dickey-Fuller test was performed [26]. Next, correlations, cross-correlations, and regressions were performed between species to evaluate relationships between major nutrient concentrations

https://doi.org/10.26434/chemrxiv-2024-gwpw5 **ORCID:** https://orcid.org/0000-0002-6737-415X Content not peer-reviewed by ChemRxiv. **License:** CC BY-NC-ND 4.0

(ortho-phosphate, total phosphorus, ammonia and nitrate/nitrite), competing ions (Ca and Mg), heavy metals (specifically Zn^{2+}), and the effect of stream pH on major nutrients and chloride compositions. The correlations, cross-correlations, and regressions were completed to assess the degree of association between species and the presence of any dynamics between species (whether past levels of one is associated with present levels of another) using standard time series analysis techniques [27]. A relationship between species within a stream was determined to be significant only if each coefficient in the regression model passed a t-test, the model residuals were stationary, and the equation yielded an R-squared or adjusted R-squared of >0.90.

2.3 Chemicals and Reactor Configuration

All electrochemical experiments in the screening analysis were conducted using synthetic wastewater which simplifies the test by eliminating the complexities associated with real wastewater, such as biological contaminants, emerging pollutants, and heavy metals. The wastewater was synthesized based on the composition from the one-year sampling period and the design of experiment outlined in Table S2. 1M stock solutions of twelve salts: ammonium formate NH_4COOH (Certified Crystalline 97 – 103%, Fisher Chemical), ammonium chloride NH_4Cl (ACS reagent 99.5%, Sigma-Aldrich), ammonium sulfate $(NH4)_2SO_4$ (Primary Standard 20.98 – 21.38%, Fisher Chemical), ammonium nitrate NH_4NO_3 (Certified ACS 98%, Fisher Chemical), sodium formate NaCOOH (ACS reagent 98%, Thermo Scientific), sodium chloride NaCl (Analytical 99.5%, Thermo Scientific), disodium sulfate decahydrate $Na_2SO_4.10H_2O$ (Analytical 99%, Thermo Scientific), sodium nitrate $NaNO_3$ (ACS reagent 98%, 98%, Thermo Scientific), magnesium chloride hexahydrate $MgCl_2.6H_2O$ (ACS reagent 99 – 102%, Sigma-Aldrich), calcium chloride $CaCl_2$ (ACS reagent 99%, Sigma-Aldrich), sodium phosphate

https://doi.org/10.26434/chemrxiv-2024-gwpw5 **ORCID:** https://orcid.org/0000-0002-6737-415X Content not peer-reviewed by ChemRxiv. **License:** CC BY-NC-ND 4.0

monobasic monohydrate $NaH_2PO_4.H_2O$ (Analytical 99+%, Acros Organics), and potassium phosphate dibasic K_2HPO_4 (ACS reagent 98%, Sigma-Aldrich), were prepared. The volume from each stock solution required to achieve the desired concentration of ions in the synthetic wastewater were determined using matrix algebra and 750 ml total of synthetic solution was prepared for each experimental run. The pH of each solution was adjusted to 6.25 for all runs using 0.4 M sodium hydroxide, NaOH (ACS grade, Pfaltz & Baner) solution to maintain the same initial pH for all screening experiments.

All experiments in the optimization analysis were conducted using real wastewater collected from Southerly Columbus WWTP anaerobic digester due to its high nutrient strength. Vacuum filtration was used to separate the suspended solids in the wastewater before the experiments.

All experiments – screening and optimization – were conducted using a bench-scale electrochemical reactor, as shown in Figure 1, operated in a batch mode. The reactor comprises a 1-liter jacketed glass vessel (Pine Research AFCELL8U3) and a sealed lid with multiple inlets for electrodes, a Luggin capillary, air sparger, overhead agitator, pH probe, and temperature sensor. The jacket enabled a controlled temperature experiment through the circulation of a cooling or heating fluid from a water circulator (Julabo DYNEO DD-200F) coupled with a temperature sensor for feedback from the reactor liquid to the circulator set point. The air sparger was connected to a zero-air gas cylinder equipped with a flow meter for continual supply of dissolved oxygen, a pH sensor (Oakton^{TM} pH electrode) was used to monitor the bulk solution throughout the experiment, and a speed rotator was used to control fluid agitation during experiments. A three-electrode design was utilized, consisting of either 316 or 304 stainless steel

https://doi.org/10.26434/chemrxiv-2024-gwpw5 **ORCID:** https://orcid.org/0000-0002-6737-415X Content not peer-reviewed by ChemRxiv. **License:** CC BY-NC-ND 4.0

(12″ × 36″ × 0.048″, McMaster-Carr) as the cathode, a saturated Ag/AgCl reference electrode, and graphite (12″ × 24″ × 0.06255″, Grainger) or AZ31 magnesium alloy foil as the anode (200 mm × 500 mm × 1 mm, Goodfellow). The stainless steel (SS) electrode was polished with silicon carbide sandpaper (600 grit) to remove any surface contaminants. Following the mechanical polishing procedure, the SS electrode was sonicated in deionized water for ten minutes to remove any remaining debris on the surface and subsequently air-dried before being used.

Figure 1: Schematic diagram of the electrochemical reactor.

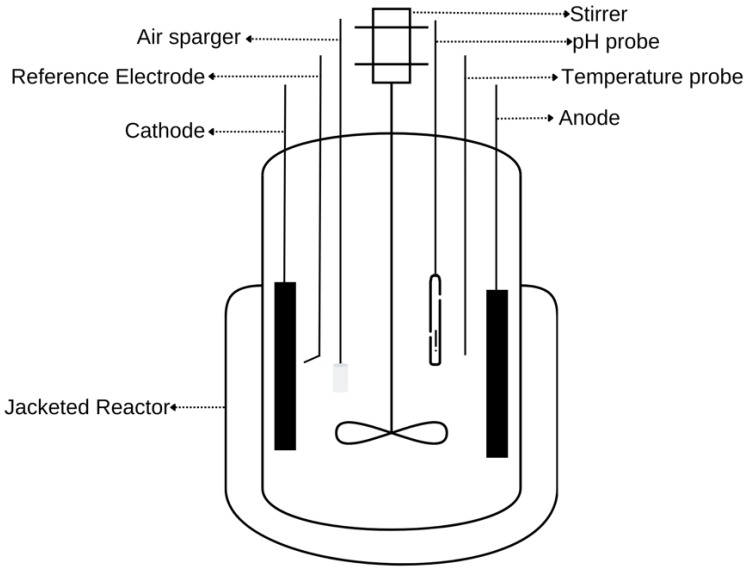

Chronoamperometric measurements – constant electrode potential, with current measured – was used to facilitate phosphate deposition by a pH increase at the cathode through water or oxygen reduction (Equations 1 and 2) depending on the potential. The cathodic potential was controlled using an Interface 5000E potentiostat (Gamry Instrument). The Luggin capillary (filled with 4M KCl) was used to position the reference electrode near the cathode to minimize ohmic resistance between the cathode and reference electrode. The anode either closes the

https://doi.org/10.26434/chemrxiv-2024-gwpw5 **ORCID:** https://orcid.org/0000-0002-6737-415X Content not peer-reviewed by ChemRxiv. **License:** CC BY-NC-ND 4.0

electrical circuit and contributes magnesium ions for nutrient recovery (equation 3) or closes the electrical circuit and does not contribute to the recovery process (equation 4). A data acquisition device (USB-1808, Measurement computing) was used to measure the overall cell voltage – potential difference between the cathode and anode – of the electrochemical system. The exposed surface area of the electrodes and the electrode type varied depending on the experimental design.

2.4 Design of Experiments and Reactor Operation

2.4.1 Screening Analyses

The eleven variables in this study, categorized into three main groups of operational, stream and design, are presented in Table 1.

Table 1: Variables in the screening analysis and their corresponding categories

Variable Category	**Variable Type**
Operational	Temperature, Turbulence, Cathodic Potential, Added Mg
Design	Anode type, Cathode type, Cathode Area to Electrolyte Volume Ratio (Area-Volume Ratio)
Stream	Initial concentrations of P, NH_4, Ca and total organic carbon (TOC)

These 11 variables were selected based on factors known to impact chemical nutrient recovery and electrochemical systems design and the variability captured from the wastewater sampling in this study. The aim of these experiments was to characterize the most influential variables affecting phosphorus recovery efficiency and specific energy consumption before attempting any process optimization. A Plackett-Burman (PB) design was chosen, which provides a first-order formulation of the system and offers the lowest number of experiments which is important when a high number of factors have been considered [28,29]. Minitab® version

https://doi.org/10.26434/chemrxiv-2024-gwpw5 **ORCID:** https://orcid.org/0000-0002-6737-415X Content not peer-reviewed by ChemRxiv. **License:** CC BY-NC-ND 4.0

21.1.0 was used to develop the PB design with ten variables at two levels each (shown in Table 2) in two blocks that accounted for the variable associated with cathode type. This design resulted in twelve distinct experimental runs, with three replicates each, in each block. The complete list of these 12 distinct experiments is provided in Table S2. The high and low levels of the stream variables were determined based on the wastewater sampling data. The operating range for the electrochemical setup was based on the prior experiments conducted in the research group [20].

Once the experiments were setup with electrodes and electrolyte in the reactor, the electrolyte was sparged with air for 30 minutes before starting the chronoamperometry experiment to saturate the solution with dissolved oxygen. Additionally, air sparging continued throughout the 6-hour experiments to sustain the dissolved oxygen level. During each experiment, 3 mL liquid samples were collected from the reactor every 30 minutes and analyzed for phosphorus content.

Table 2: Two levels of each variable in the Plackett-Burman design

Variable	**Low level**	**High level**
Temperature (°C)	10	40
Turbulence (rpm)	50	400
Cathodic potential (V vs Ag/AgCl)	-0.8	-1.3
Area-volume ratio (1/cm)	0.07	0.14
Anode type[a]	Graphite	Magnesium
Cathode type[a]	SS 304	SS 316
Mg added (ppm)	0	350
NH_4 Initial Concentration (ppm)	0	1000
P Initial Concentration (ppm)	37	300
TOC Initial Concentration (ppm)	24	200
Ca Initial Concentration (ppm)	28	162

[a]These are categorical variables

Subsequent statistical analysis was performed in Minitab using an assumed linear regression models with derived coefficients for each variable, representing the extent and

https://doi.org/10.26434/chemrxiv-2024-gwpw5 **ORCID:** https://orcid.org/0000-0002-6737-415X Content not peer-reviewed by ChemRxiv. **License:** CC BY-NC-ND 4.0

direction of the change in the mean value of the response when each factor is individually altered, and derived coefficient variability represented by its standard deviation (SD) [30]. Factors with a *P*-value lower than the significance level (α) of 0.05 were important variables and the *t*-value, calculated as the ratio of the coefficient to its SD is illustrated in a descending order as a Pareto chart of standardized effects [29–31]. This chart establishes the order of the variable significance, with those exceeding the reference line considered as the key factors [32]. The linear regression models were also characterized by the R-squared value, with higher values indicating a better model accuracy. Additionally, normal probability plot of residuals assessing the goodness of fit for the proposed models were also acquired, which should have a linear trend to verify the normal distribution of residuals [33]. Finally, Kernel Density Estimation (KDE) with a bandwidth of 0.1 was used to compare the performance of SS316 and SS304 in each experiment block in terms of both responses. A KDE distribution visualizes the data spread and the abundance of each value compared to the other values in the population [34], and in this study, the performance of the two SS types in terms of the overall performance and data spread tendency were compared using this type of plot.

2.4.2 Optimization Analysis

The optimization analysis was conducted to determine the optimal operating conditions for ENR based on three down-selected variables from the screening analysis with more test points added for these three variables. The circumscribed version of a Box-Wilson central composite design (CCD) was selected, comprising 8 corner points, 6 axial points, and 6 center points with two replicates each. CCD is a common response surface method for second-order modeling, mainly due to the efficient number of experimental runs required [29] and its ability to explore

https://doi.org/10.26434/chemrxiv-2024-gwpw5 **ORCID:** https://orcid.org/0000-0002-6737-415X Content not peer-reviewed by ChemRxiv. **License:** CC BY-NC-ND 4.0

extreme input variable values through the axial points. The second-order model captures the curvature in the response (i.e., the interaction between variables and quadratic effects), and was used in combination with the response optimizer in Minitab to quantify the conditions that maximize percentage phosphorus recovery and minimize specific energy consumption. The actual factors and levels of the experimental design are presented in Table S3 while a full list of the distinct experimental runs is shown in Table S4. The center point is the midpoint value between the high and low values from the screening analysis, the corner points are the refined high and low values for this analysis, while the axial points are the extreme high and low values calculated from the center point using an axial spacing of 1.633. The reactor operation was similar to the screening analysis; however, the chronoamperometry experiments were conducted over 2 hours, as the recovery from the real wastewater samples occurred more quickly. Additionally, 3 mL liquid samples were collected periodically and analyzed for phosphorus content.

2.5 Material Characterization

2.5.1 Liquid Characterization

All liquid samples were analyzed for phosphorus concentration with an Inductively Coupled Plasma – Optical Emission Spectrometer (ICP-OES, iCAP 6000 Series, Thermo Scientific, USA) at a wavelength of 185.891 in axial mode. The ICP-OES is an analytical technique that relies on ions' ability to be excited and emit electromagnetic radiation at a wavelength specific to an element [35]. The instrument was calibrated using a standard solution with concentrations within the range of the expected levels in the wastewater samples. For sample preparation, the liquid was centrifuged to remove any precipitated solids that could clog the tubes transporting the fluid in and out of the instrument. The clarified samples were then

https://doi.org/10.26434/chemrxiv-2024-gwpw5 **ORCID:** https://orcid.org/0000-0002-6737-415X Content not peer-reviewed by ChemRxiv. **License:** CC BY-NC-ND 4.0

diluted tenfold with deionized water in a 10 ml (±0.08) volumetric flask to prepare them for analysis.

2.5.2 Solid Characterization

After each experiment, the electrodes were air-dried for 24 hours, while the precipitates from the bulk solution were filtered, air-dried, and stored under ambient conditions. Scanning Electron Microscopy (SEM, JEOL JSM 6010PLUS/LA) was used to examine the morphology of the solids, while X-ray Dispersive Spectroscopy (EDS) coupled with the SEM with an accelerating voltage of 15 kV and working distance (WD) of 11 mm, was used to determine the elemental composition and particle size measurements were performed using ImageJ software [36]. X-Ray Diffraction (XRD, Rigaku miniflex 600) was used for phase identification and composition of the solids using Cu-Kα radiation (1.54059 Å), a 2θ range of 10-90 degrees, a speed of 2.5 deg/min, a step angle of 0.02°, a current of 15 mA and a voltage of 30 kV. The refinement of the collected diffractograms were performed via GSAS-II program [37], using the Rietveld method [38]. Crystallographic texture, instrument parameters, sample displacement, phase fractions, lattice parameters and background signal are parameters that were refined from the raw data. A data residual value (R_w), indicating the difference between the raw and refined diffractograms of the sample [39] is calculated at the end of each refinement and an R_w value in or close to the range of 5-10 % is considered a good agreement.

2.6 Figures of Merit

The electrolyzer's performance was characterized by the phosphorus recovery percentage/efficiency and specific energy consumption (kWh/kg P), which are two of the critical

https://doi.org/10.26434/chemrxiv-2024-gwpw5 **ORCID:** https://orcid.org/0000-0002-6737-415X Content not peer-reviewed by ChemRxiv. **License:** CC BY-NC-ND 4.0

figures of merit relevant to this nutrient recovery approach[40]. The equations of these responses are represented in Equations 5 and 6, respectively:

$$\text{P \% recovery} = \frac{C_0 - C(t)}{C_0} \times 100\% \quad (5)$$

$$E_s = \frac{\int E(t)I(t)dt}{V(C_0 - C(t))} \quad (6)$$

where C_0 is the initial P concentration (in ppm), C(t) is the P concentration at time t (in ppm), E(t) is the cell voltage at time t (in V), I(t) is the total current at time t (in A) and V is the volume of electrolyte or wastewater in the reactor (in L). Phosphorus concentration data obtained from ICP-OES was used to calculate the percentage recovery, while a combination of data from ICP-OES, potentiostat and data acquisition device was used to compute the specific energy consumption.

3 Results and Discussion

3.1 Municipal Wastewater Sampling

3.1.1 Concentration of Total Phosphorus

The 1-year sampling analyses of the three streams are summarized as box plots in Figure 2, showing the significant variations in the composition of the three wastewater streams, attributable to differences in influent composition, solids concentration fed into the digesters [41] and treatment stages as well as the associated efficiencies of these treatment stages.

https://doi.org/10.26434/chemrxiv-2024-gwpw5 **ORCID:** https://orcid.org/0000-0002-6737-415X Content not peer-reviewed by ChemRxiv. **License:** CC BY-NC-ND 4.0

Figure 2: Boxplot showing the concentration of (a) phosphorus (b) ammonia (c) nitrate-nitrite (d) calcium (e) magnesium (f) total organic carbon in Southerly Columbus Ohio WWTP (100 MGD) Anaerobic dewatering effluent and Thickening effluent together with Athens Ohio WWTP (4 MGD) Aerobic effluent.

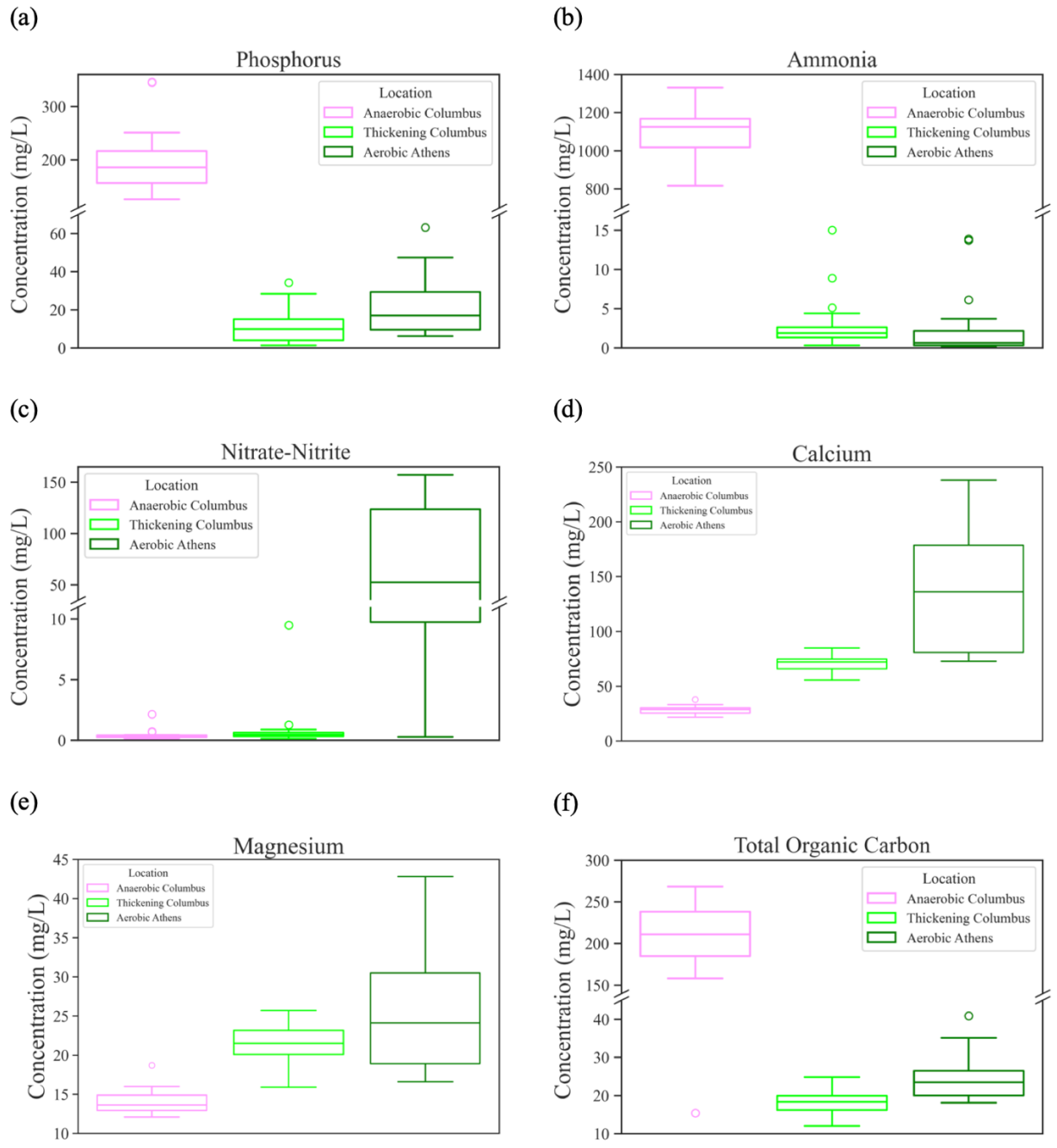

https://doi.org/10.26434/chemrxiv-2024-gwpw5 **ORCID:** https://orcid.org/0000-0002-6737-415X Content not peer-reviewed by ChemRxiv. **License:** CC BY-NC-ND 4.0

Aerobic digesters, typical of smaller WWTPs such as Athens, Ohio WWTP, use microorganisms in waste-activated sludge (WAS) to break down organic matter in the presence of oxygen. These microorganisms consume phosphorus for their growth and retain it in the biosolids, resulting in a lower P content in the effluent [10,41]. In contrast, the anaerobic digesters in larger treatment plants usually produce effluent with high nutrient content. These digesters use methane-producing bacteria, which require less nutrients for their growth, to break down the sludge's organic content in an oxygen-free environment [41]. Additionally, in WWTPs with an enhanced biological phosphorus removal (EBPR) step such as the Southerly Columbus plant, anaerobic digestion releases phosphorus accumulated in the feed sludge by phosphorus-accumulating organisms (PAOs) in the EBPR process[41], further increasing the P concentration in the supernatant. Before anaerobic digestion, thickening centrifuges are used to reduce the liquid volume of WAS to be fed to the digester. Therefore, the effluent from this process is expected to have lower P concentration.

The phosphorus concentration in the aerobic effluent sample collected from Athens Ohio WWTP ranges from 6 to 63 mg/L, correlating with aerobic filtrate characteristics observed in some WWTPs in North Florida as reported by Hallas *et al.* [42]. The total P content in the anaerobic effluent from Southerly Columbus Ohio WWTP ranges from 126-346 mg/L, consistent with the average concentration reported by Lee *et al.* and Wang e*t al.* [43,44]. Also, the phosphorus concentration in the thickening effluent, falls below the upper limit of 60 mg/L reported by Metcalf *et al.* [41], ranging between 1.32 - 34.24 mg/L. This slight variation from the upper limit might be due to lower P content in the plant's influent stream or the efficiency of P removal treatment before centrifuge thickening.

https://doi.org/10.26434/chemrxiv-2024-gwpw5 **ORCID:** https://orcid.org/0000-0002-6737-415X Content not peer-reviewed by ChemRxiv. **License:** CC BY-NC-ND 4.0

3.1.2 Concentration of Ammonia-Nitrogen, Nitrate-Nitrite

Nitrogenous compounds in wastewater treatment plants are usually found as free ammonia (NH_3 and its ionized form, ammonium NH_4^+), nitrate (NO_3^-), nitrite (NO_2^-), and organic nitrogen [45]. Figures 2b and 2c illustrate the concentration of free ammonia and nitrate-nitrite, respectively, across the three wastewater samples. Typically, nearly all free ammonia exists as ammonium at room temperature and a pH of around 7 [46]. In the anaerobic effluent sample with an average pH of 7.16, the free ammonia concentration (Figure 2b) aligns with typical anaerobic supernatant ammonium levels ranging from 800 to 1300 mg/L, as reported by Metcalf *et al.* [41]. This suggests that almost all free ammonia in the Columbus anaerobic sample exists as ammonium, making it less toxic.

In a typical WWTP, ammonium in the mainstream is removed by oxidation to nitrate through nitrification, facilitated by specific bacteria in the presence of oxygen. Subsequently, reduction of the nitrate to nitrogen gas occurs through denitrification. However, during anaerobic sludge treatment, organic nitrogen in the sludge is broken down into ammonium, which does not nitrify due to lack of oxygen in the digesters. This explains why the anaerobic effluent ammonium concentration in Figure 2b is notably higher, and the nitrate-nitrite concentration in Figure 2c is comparatively lower than in the aerobic effluent. The ammonium and nitrate-nitrite concentration in the thickening effluent falls within the lower range of data reported in existing literature (0-45 mg-NH_4/L, 0-30 mg-NO_x/L) [41]. These concentrations are potentially influenced by the amount of wash water used in the thickening centrifuges.

https://doi.org/10.26434/chemrxiv-2024-gwpw5 **ORCID:** https://orcid.org/0000-0002-6737-415X Content not peer-reviewed by ChemRxiv. **License:** CC BY-NC-ND 4.0

3.1.3 Concentration of Calcium and Magnesium

Ionic species such as Ca^{2+} and Mg^{2+}, often used as indicators of water hardness, provide insights into the scaling potential of WWTPs [47]. Furthermore, these cations play a role in estimating the nutrient recovery potential from wastewater due to their ability to react with phosphate and ammonium. Figures 2d and 2e show the concentrations of Ca and Mg, respectively, present in the sampled wastewater.

The concentration of calcium in the anaerobic effluent from Southerly Columbus ranges from 22 to 38 mg/L, whereas in the aerobic effluent from Athens, it fluctuates between 73 and 240 mg/L. The hardness of drinking water in the city of Athens, 146 mg/L [48] is higher, on average, than that in the city of Columbus 92-125 mg/L on an annual basis [49]. This difference in water hardness may contribute to the observed differences in calcium concentration between the two WWTPs. The higher calcium concentration in the Athens samples, coupled with the low ammonium ions concentration shown in Figure 2b, suggests that phosphorus recovery via calcium-based phosphates, such as hydroxyapatite ($Ca_{10}(PO_4)_6(OH)_2$) is a more feasible route than magnesium-based phosphates e.g. struvite ($NH_4MgPO_4.6H_2O$) precipitation in this treatment plant. Conversely, the low calcium concentration in Columbus anaerobic effluent indicated that the impact of Ca as a competing ion for phosphate recovery through struvite precipitation may be negligible, provided there is sufficient Mg available for the reaction.

Furthermore, a Mg:Ca molar ratio of about 2 or higher is required for fast struvite growth and a short induction time [50]. Ojoawo and Daramola have also reported the significance of a Mg:Ca molar ratio of 2.1 for efficient electrochemical phosphorus recovery from animal wastewater [24]. According to Figure 2e, the magnesium concentration in the anaerobic effluent is

https://doi.org/10.26434/chemrxiv-2024-gwpw5 **ORCID:** https://orcid.org/0000-0002-6737-415X Content not peer-reviewed by ChemRxiv. **License:** CC BY-NC-ND 4.0

lower than that in the aerobic effluent, initially suggesting that more external Mg would be required for struvite precipitation in the anaerobic effluent, without considering the ammonium content. However, a more detailed examination of the Mg:Ca molar ratios in the two samples shows that the anaerobic effluent has an average of 0.82 compared to 0.31 in the aerobic effluent. This implies that a lesser amount of Mg is required to achieve the reported Mg:Ca molar ratio conducive for efficient struvite recovery in the anaerobic effluent compared to aerobic effluent.

3.1.4 Organic Content (Total Organic Carbon)

Figure 2f presents the concentration levels of total organic carbon in the three sampled wastewater sources. The presence of organic matter in wastewater, such as organic carbon, can adversely impact the nucleation and growth of phosphate precipitate such as struvite, by blocking active growth sites of the struvite nuclei due to the coprecipitation of organic matter [51]. Therefore, it is important to assess the impact of TOC on P recovery from municipal wastewater due to its complex matrix. Extensive literature data on the TOC concentration of post-digester municipal wastewater is lacking. However, untreated wastewater influent typically contains about 109-328 mg/L TOC, while activated sludge with biological nutrient removal (AC-BNR) effluent tends to have approximately 10-20 mg/L TOC [41]. A comparison of this data with Figure 2f suggests that a substantial portion of the organic carbon removed during secondary treatment (i.e. AC-BNR) is released after anaerobic digestion which has a supernatant with TOC concentration ranging from 166-270 mg/L. Columbus thickening process, which reduces activated sludge volume before anaerobic digestion, has an effluent TOC concentration between 12-25 mg/L, consistent with the AC-BNR values. Athens WWTP, a conventional activated sludge plant, has an aerobic effluent with TOC concentration between 18-41 mg/L, similar to values reported by Metcalf et *al.* [41].

https://doi.org/10.26434/chemrxiv-2024-gwpw5 **ORCID:** https://orcid.org/0000-0002-6737-415X Content not peer-reviewed by ChemRxiv. **License:** CC BY-NC-ND 4.0

3.1.5 Heavy Metals

It is important to also consider that municipal wastewater contains pollutants such as heavy metals, which could co-precipitate with phosphate compounds, and limit its use as a fertilizer. Heavy metal contaminants such as arsenic, cadmium, chromium, mercury, lead, and others can be toxic based on continuous exposure over a long period. For instance, long-term exposure to lead causes mental impairment, cadmium has adverse effects on the kidney, liver, and gastrointestinal tract, while arsenic can lead to skin poisoning [52]. Moreover, the remediation of soils contaminated with heavy metals is a highly costly process; therefore, prevention of pollution caused by heavy metals is important [52]. Table S5 presents the average concentrations of heavy metals in the effluents in comparison with the EPA's maximum limits for heavy metals in sludge intended for to soil application. The data from the table shows that the concentration of heavy metal pollutants in the liquid portion of the wastewater streams are within the parts per billion range, significantly lower than the EPA's ppm thresholds for sludge.

3.1.6 Time Series Analyses

Given the variability in the wastewater compositions, time series analyses were used to explore correlations among pH, nutrient levels, ionic and heavy metals species, and how they changed with respect to each other over the one-year sampling period. Each species' time series data was first tested for stationarity with stationarity defined as an integration value of zero (0) for a stationary data series (the mean, variation, and autocorrelation structure do not change with time) and integration value of one (1) for a time series that is non-stationary. A summary of the integration values of each species in each of the three streams is given in Table S6.

https://doi.org/10.26434/chemrxiv-2024-gwpw5 **ORCID:** https://orcid.org/0000-0002-6737-415X Content not peer-reviewed by ChemRxiv. **License:** CC BY-NC-ND 4.0

Based upon correlations, cross-correlations, and regressions between various stream species (within each individual stream), four major findings were concluded from the time series analyses: 1) Ortho-P and ammonia did not exhibit a significant relationship in any stream tested, 2) there exist relationships between Ca, Mg, and Ortho-P in the Columbus anaerobic and Athens aerobic streams, 3) Zn^{2+} showed no significant relationship with respect to nutrients in any stream tested, and 4) stream pH is related to both Ortho-P and Cl concentrations in the Columbus anaerobic and Athens aerobic streams.

In general, the Columbus thickening stream exhibited differing behavior from the two other streams. Equations 7 and 8 below are the regression equations found to best fit the relationship between Ca and Ortho-P (denoted P_{Ortho}) in the Columbus anaerobic stream and the Athens aerobic stream, respectively. Note that the differenced stream species concentration (Δ) must be used when determining relationships between species with different integration values (Table S6), with the (Δ) being applied to the species having the higher integration value. The time variable (t) denotes the sample time interval (two weeks in this study) and thus, t is in units of 2 weeks. All concentrations are in ppm and pH is reported in standard pH units.

$$Ca(t) = 0.951 \times Ca(t-1) - 0.0882 \times \Delta P_{Ortho}(t) + 0.0684 \times \Delta P_{Ortho}(t-1) \quad (7)$$

$$Ca(t) = 0.644 \times Ca(t-1) + 2.006 \times P_{Ortho}(t) \quad (8)$$

The Athens aerobic stream also exhibited significant relationships between Mg and Ortho-P (Equation 9) and Ca and Mg (Equation 10). Similar relationships for the Columbus anaerobic stream were determined to be insignificant.

$$Mg(t) = 0.3109 \times P_{Ortho}(t) + 0.712 \times Mg(t-1) \quad (9)$$

$$Ca(t) = 0.8797 \times Ca(t-1) + 6.36 \times Mg(t) - 5.744 \times Mg(t-1) \quad (10)$$

https://doi.org/10.26434/chemrxiv-2024-gwpw5 **ORCID:** https://orcid.org/0000-0002-6737-415X Content not peer-reviewed by ChemRxiv. **License:** CC BY-NC-ND 4.0

The pH values of Columbus anaerobic and Athens aerobic streams were determined to be dependent on both Ortho-P and Cl concentrations. Equations 11 and 12 below show these relationships for the Columbus anaerobic stream while Equations 13 and 14 describe the Athens aerobic stream. Note that the following regressions are in log-based pH units and therefore have small regression equation coefficients. Completing the analysis on a proton concentration basis did not change the resulting relationships.

$$pH(t) = 0.9959 \times pH(t-1) + 0.0026 \times \Delta P_{Ortho}(t) - 0.0036 \times \Delta P_{Ortho}(t-1) \quad (11)$$

$$pH(t) = 0.9771 \times pH(t-1) + 0.001565 \times \Delta Cl(t) \quad (12)$$

$$pH(t) = 1.0123 \times pH(t-1) - 0.0357 \times P_{Ortho}(t) + 0.0319 \times P_{Ortho}(t-1) \quad (13)$$

$$pH(t) = 0.7541 \times pH(t-1) + 0.01138 \times Cl(t) \quad (14)$$

These general results can be used to frame the considerations necessary when developing a side-stream P recovery system for a specific WWTP. First, because Ortho-P and ammonia behaved independently of one another within the tested streams, a system designed for struvite recovery may necessitate monitoring of both nutrients. Also, if a thickening stream is to be used for P recovery, separate considerations will be necessary as the thickening stream had very little interdependence among its stream species concentrations. Finally, it was shown that major ions (Ca and Mg) exhibit an interdependence on nutrient concentrations (Ortho-P) and stream pH is interdependent with Ortho-P and Cl in both post-digester streams i.e., the Columbus anaerobic and Athens aerobic streams. These relationships may be leveraged to simplify sensing or process controls to adjust stream chemistry for efficient P recovery. Lastly, recognizing the differences between the digesters that these streams flow out from: anaerobic for Columbus versus aerobic

https://doi.org/10.26434/chemrxiv-2024-gwpw5 **ORCID:** https://orcid.org/0000-0002-6737-415X Content not peer-reviewed by ChemRxiv. **License:** CC BY-NC-ND 4.0

for Athens stream, suggest further investigations into the biological processes within these digester types could be beneficial for understanding the compositional variability for nutrient recovery applications.

3.2 Evaluation of the Key Variables in Electrified Nutrient Recovery

3.2.1 Screening of Significant Variables for P % Recovery

The regression models and associated R-squared values, evaluating the relationship between the variables and system responses are shown in Table S7 and Table S8, for SS316 and SS304, respectively. The statistical parameters for these linear regression models are provided in Table S9 (SS316) and Table S10 (SS304), while the normal probability plots of the residuals for SS316 and SS304 are shown in Figure S2a and Figure S2b, respectively. The R-squared values are 0.98 and above, and the residual of the models follow a straight line, indicative of the model's reliability. After performing the statistical screening analysis, the Pareto chart of the standardized effects for both SS types are shown in Figure 3a and Figure 3b.

https://doi.org/10.26434/chemrxiv-2024-gwpw5 **ORCID:** https://orcid.org/0000-0002-6737-415X Content not peer-reviewed by ChemRxiv. **License:** CC BY-NC-ND 4.0

Figure 3: Pareto chart of the standardized effects for a) P % recovery of SS316, b) P % recovery of SS304, c) ln(Es) of SS316, and d) ln(Es) of SS304. The black bars represent a variable with a direct proportionality to the response, while grey bars represent an inverse proportionality. In the case of anode type (a categorical variable), black bars represent a high response value and grey bars represent a low response value, both based on the magnesium anode (the reverse relationships would be for a graphite anode).

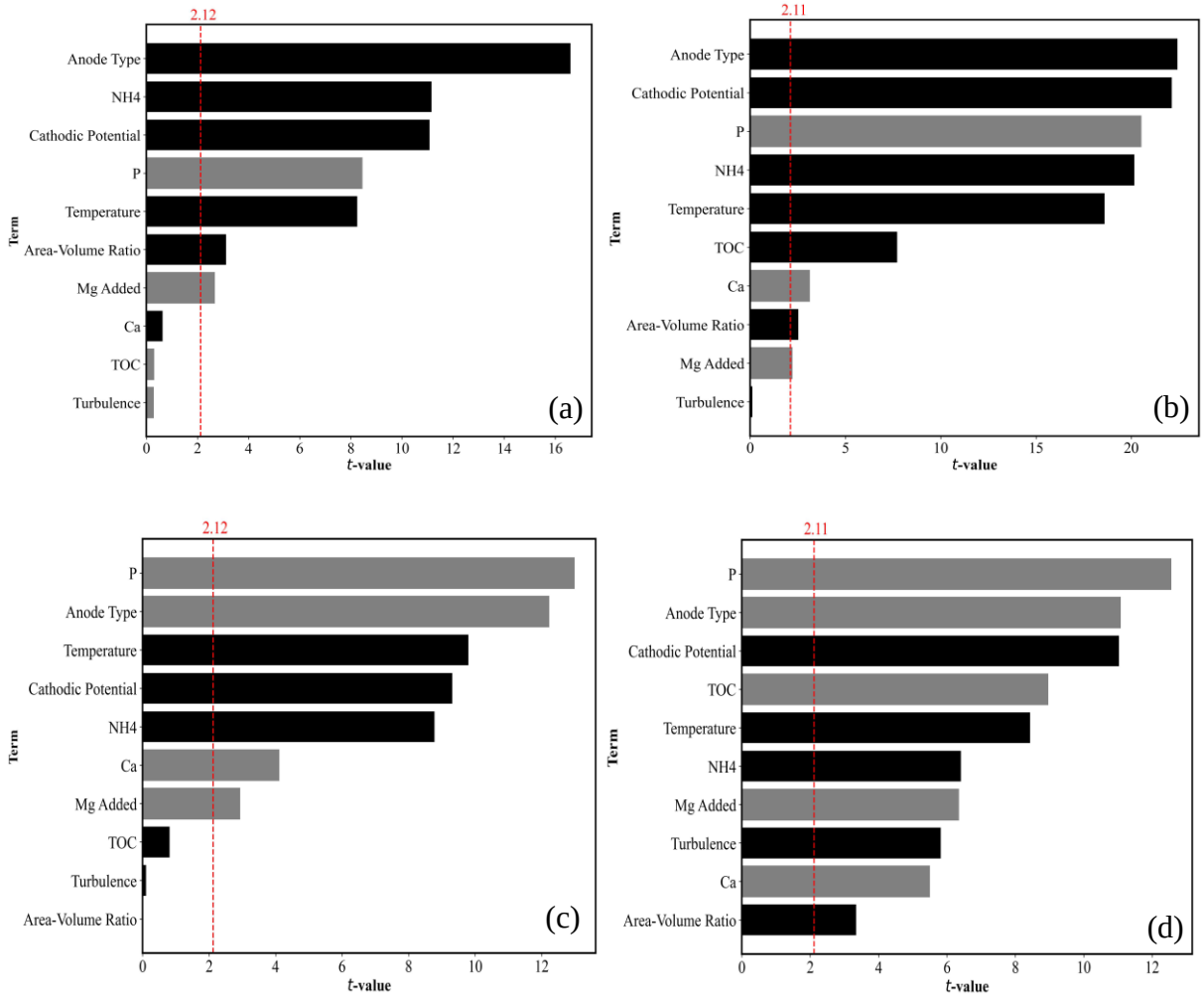

For SS316, seven out of ten variables had a significant influence. However, the first five factors in Figure 3a with *t*-values at least three times the threshold of 2.12, had more pronounced

https://doi.org/10.26434/chemrxiv-2024-gwpw5 **ORCID:** https://orcid.org/0000-0002-6737-415X Content not peer-reviewed by ChemRxiv. **License:** CC BY-NC-ND 4.0

effects on the P % Recovery. These variables in the order of importance are anode type, NH_4 concentration, cathodic potential, P concentration and temperature. In the SS304 block, all variables except for turbulence were significant. Similarly, in this block, emphasis was placed on the variables that have a more significant impact on the response, specifically those with a *t*-value exceeding three times the threshold of 2.11. These variables are anode type, cathodic potential, P concentration, NH_4 concentration, temperature and TOC, respectively. As it can be noticed from the list of the key variables in the two blocks, regardless of the order, there are five overlapping important factors for both SS316 and SS304. However, it is noteworthy that each block exhibits its unique magnitude of variable effects, and no single factor exerts identical influence on both SS types. Despite the difference in the magnitude of the effects, using a Mg anode (as opposed to a graphite anode), along with the presence of NH_4, a more negative cathodic potential and a higher temperature each led to an increased P recovery for both SS cathodes. Conversely a higher initial concentration of P (300 ppm) yields a lower percentage recovery, although the absolute quantity of P recovery in ppm was generally higher. For example, a 37 ppm initial P concentration with a 100 % P recovery will give only 28 mg of recovered P while a 300 ppm initial P with recovery as low as 15% gives 34 mg of recovered P.

The literature supports the higher P recovery by using an Mg anode and solutions with higher NH_4 concentration; furthermore, high N:P ratios promote struvite precipitation, which is one of the methods of P recovery [19,53,54]. Lui et *al*. showed a directly proportional relationship between temperature and P recovery for P concentrations below 400 ppm, which is consistent with the findings of this study [55]. However, some studies with a focus on P recovery as struvite, reported a higher P recovery at lower temperatures [54,56,57]. This can be explained by considering the presence of other P-containing products apart from struvite in the screening experiments i.e.,

https://doi.org/10.26434/chemrxiv-2024-gwpw5 **ORCID:** https://orcid.org/0000-0002-6737-415X Content not peer-reviewed by ChemRxiv. **License:** CC BY-NC-ND 4.0

while struvite recovery is improved at lower temperatures, other P-containing solids have improved recovery at higher temperatures. Lastly, more negative cathodic potentials are reported in literature[58] to result in higher P recoveries, by producing more OH^- ions due to the Equation 1 or 2, thereby increasing the pH and facilitating the precipitation of P-containing compounds.

Apart from the five variables discussed above, initial TOC is a key factor with a directly proportional effect on P % recovery for SS304, however, it was found unimportant for SS316. One category of organic carbon is natural organic matter (NOM). This group contains decomposed humic and nonhumic substances with heavy, long chain molecules and several functional groups [59]. Lei et *al*. showed the presence of natural organic matter (NOM) increased the P recovery by coprecipitation with calcium phosphate [60]. Conversely, Wang et *al*. suggested that if the product of interest is struvite, organic compounds with smaller molecular weights offer higher P recovery with better product purity [61]. Considering the TOC in this synthetic water analyses was the formate ion, which is smaller than a typical heavy organic carbon present in municipal wastewater, the directly proportionality between TOC and P recovery could be explained by the possibility of P mostly recovered as struvite. However, this hypothesis is more likely for the cases where the concentration of Mg in the stream is higher than Ca.

3.2.2 Screening of Significant Variables for ln (E_s)

Given the substantial disparity in the E_s magnitudes as seen in Figure S3, the screening analysis was conducted using the natural logarithm (ln) of E_s instead of the original values to linearize the response and reduce the distance between the data points. This is beneficial considering the regression analyses in the screening section is based on a combination of linear terms and distant data values might potentially increase the error in the model's prediction. The

https://doi.org/10.26434/chemrxiv-2024-gwpw5 **ORCID:** https://orcid.org/0000-0002-6737-415X Content not peer-reviewed by ChemRxiv. **License:** CC BY-NC-ND 4.0

results of the statistical analysis on E_s for SS316 are displayed in Figure 3c and Table S11, while the normal probability plot for the regression model is in Figure S2c. The same information for SS304 is shown in Figure 3d, Table S12, and Figure S2d. Among the ten variables evaluated, seven had significant impact on E_s in the SS316 block, with the first five factors in the Pareto chart exerting the most noticeable impact, having a *t*-value more than three times the threshold of 2.12. These variables were initial P concentration, anode type, temperature, cathodic potential and NH_4 concentration, respectively. In the SS304 block, all variables were recognized to be influential on E_s and seven of these variables were most noticeable, with a *t*-value greater than three times the threshold (2.11). Consequently, the overlapping important factors in both SS316 and SS304 with a *t*-value over three times the threshold are initial P concentration, anode type, cathodic potential, NH_4 concentration and temperature.

A higher initial P and an Mg anode resulted in a decrease in E_s. On the other hand, a graphite anode, a more negative cathodic potential, the presence of NH_4 and a higher temperature increased E_s. It is important to acknowledge that in Equation 6, the denominator is the mass of the recovered product. As explained in the previous section, a higher initial phosphorus concentration will most likely result in a greater mass of the product. This, in turn, increases the denominator value in Equation 6. On the other hand, the numerator in this formula is the actual energy consumed which is the integral of the product of the cell voltage and generated current. Therefore, increasing the concentration of phosphate ions will result in lower ionic resistance and higher current, therefore potentially increasing the numerator. However, it is plausible that the denominator has a higher order of increase in comparison to the numerator, resulting in an overall decrease in the E_s with a higher initial P. Higher E_s has also been observed in electrochemical nutrient recovery using streams with lower initial P concentration in literature [58].

https://doi.org/10.26434/chemrxiv-2024-gwpw5 **ORCID:** https://orcid.org/0000-0002-6737-415X Content not peer-reviewed by ChemRxiv. **License:** CC BY-NC-ND 4.0

Additionally, a smaller E_s with utilization of an Mg anode could be attributed to a smaller magnitude of the average cell voltage using this anode (typically 2V less than the graphite anode), and higher mass of recovered product obtained as explained in the previous section. This would result in lower energy consumption as defined in Equation 6.

A more negative applied cathodic potential is expected to increase the average cell voltage and generated current. On the other hand, this more negative applied potential also increases the P % recovery, *vide supra*, which does not necessarily translate to a higher amount of recovered P in all cases. Consequently, it is possible that the more negative potential will exert a more pronounced positive effect on the numerator of the E_s formula, resulting in an overall increase in E_s. Wang et *al.* also observed an increase in the E_s with a more negative applied potential [58]. As for the NH_4 concentration, the presence of this ion increases the P % recovery, but not necessarily the amount of P recovered. On the other hand, the presence of 1000 ppm of this ion in the electrolyte could aid in increasing the generated current due to decreased electrolyte resistance. It is possible that this high concentration of NH_4 could increase the current more significantly than increasing the ppm P recovered and therefore due to the Equation 6, causing an overall increase in E_s.

Finally, a higher temperature will result in an increased Mg corrosion in water as described in Equation 3[62], which concurrently increases the pH, based on the ability of sacrificial magnesium to also enhance the cathodic reaction for hydroxide generation[63]. This higher pH leads to greater precipitation by shifting the equilibrium for phosphate speciation towards anions that precipitate: HPO_4^{2-} and PO_4^{3-}. On the other hand, a higher temperature also facilitates improved reaction kinetics and ion mobility resulting in an increased generated current. Consequently, the positive effect of higher temperature on the current could be more significant

https://doi.org/10.26434/chemrxiv-2024-gwpw5 **ORCID:** https://orcid.org/0000-0002-6737-415X Content not peer-reviewed by ChemRxiv. **License:** CC BY-NC-ND 4.0

than the recovered product, resulting in a directly proportional relationship between temperature and E_s.

3.2.3 Comparison of SS316 and SS304 Performances

Figure 4a depicts P % Recovery KDE distributions for each SS type. Comparing these graphs reveals a comparable overall spread of data and curve behavior for both SS blocks, with a notable exception: in the range of approximately 40-80% recovery, SS304 showed no recovery activity. Furthermore, upon closer examination of the bar graph presented in Figure 4b, it is evident that experiment types 11 and 12 exhibit a more significant difference between the two cathode types with no overlap in the uncertainties and SS316 providing higher recoveries. Given the superiority of SS316's corrosion resistance compared to SS304 in chloride solutions due to a slower dissolution of the oxide passive film on the surface [64] and considering that the electrolyte contains more than 300 ppm of Cl^- in all experiments, it is conceivable that SS304 might have experienced diminished stability, leading to a compromised performance in experiment types 11 and 12.

Figure 4: a) Kernel Density plots of SS316 and SS304 for P % recovery with a low bandwidth and b) Bar charts of P %recovery range for SS316 and SS304.

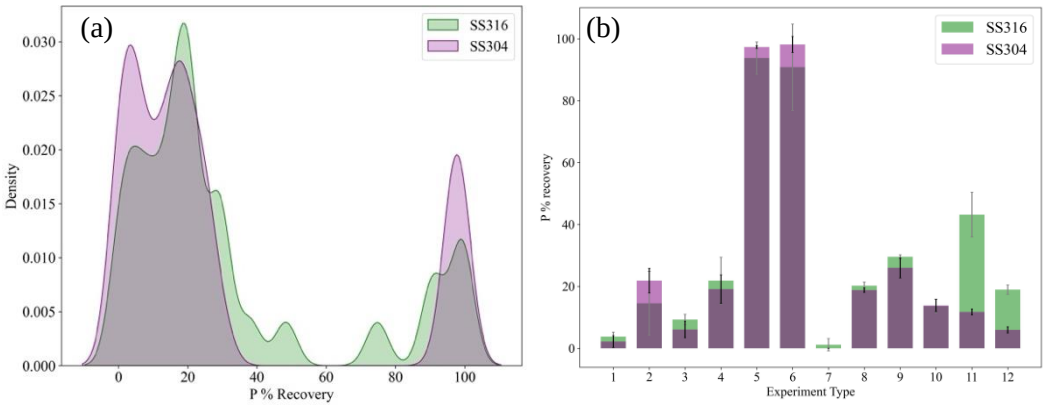

https://doi.org/10.26434/chemrxiv-2024-gwpw5 ORCID: https://orcid.org/0000-0002-6737-415X Content not peer-reviewed by ChemRxiv. License: CC BY-NC-ND 4.0

In experiment type 11, temperature and cathodic potential are low, while P initial concentration is high. By comparing the magnitudes and direction of effects in the Pareto charts in Figure 3a and Figure 3b, it is evident that even though the direction of the effects for these three factors are the same in both SS blocks, but they have a more pronounced impact (higher *t*-values) on the response for SS304. This implies that a less negative cathodic potential and lower temperature, along with a higher initial P, decrease SS304's P recovery to a greater extent than SS316's P recovery. However, the individual factors also have interactions themselves, e.g. low temperature may lead to slower kinetics, and the combination of a low temperature with low applied potential and low agitation could introduce a much lower P recovery. Therefore, under conditions where all the factors have a significant effect i.e., SS304 as opposed to SS316, the combined effect on P recovery is more pronounced.

On the other hand, experiment 12 involves a low cathodic potential, a small area-volume ratio, no NH_4, and a high initial P. The same scenario applies here: factors that are inversely impacting the P recovery exert a more negative impact on the SS304's response and the potential interaction between these variables might make this inhibition even stronger in SS304 as opposed to SS316. Moreover, as illustrated in Figure S4 the KDE distributions for ln (Es) of each SS type indicate dissimilar trends between these two cathode types, providing additional evidence of distinct electrochemical behaviors in each of these respective cases. As evident from Figure S3, SS304 has lower E_s magnitudes and due to the comparable P recoveries in most cases for the two SS types (denominator of Equation 6), the lower E_s in the SS304 case with the same applied potential, could be due to lower current generated. This may be attributed to a less current generated in this SS type due to a possible diminished electrical property in an environment containing Cl^- [64].

https://doi.org/10.26434/chemrxiv-2024-gwpw5 **ORCID:** https://orcid.org/0000-0002-6737-415X Content not peer-reviewed by ChemRxiv. **License:** CC BY-NC-ND 4.0

3.2.4 Screening Summary and Transitioning Toward Optimization

Overall, regardless of the magnitude of the effects, the same five key factors emerge as significant for both SS types for P % recovery and E_s responses: anode type, cathodic potential, initial P and NH_4 concentration and temperature. Therefore, an optimization analyses for nutrient recovery with P % recovery and E_s as the key responses focused on these five variables. The electrolyte that provides the most significant opportunity for recovery, based on high nutrient contents was the anaerobic digester effluent which provided a source of real wastewater but negates the ability to vary nutrient concentrations. Furthermore, considering the anode type is the most important variable and the Mg anode favors a desired outcome in both responses – high amount of P recovered and low energy consumption – Mg was the anode in the optimization experiments. SS304 was chosen as the cathode over SS316, since both cathodes yielded a comparable level of P recovery in over 80% of the experiments (Figure 4) and SS304 is less costly than SS316. These conditions simplified our number of independent factors from 5 to 2: temperature and cathodic potential. The electrode size was included as the third variable since it was a variable above the threshold of significance in both electrodes (Figure 3) and this value provides significance in evaluating cost analyses for the Mg anode. Therefore, the optimization analysis with respect to the electrode area places emphasis on identifying the optimum size rather than merely selecting the maximum size.

3.3 Optimization of the P Recovery from Real Wastewater

3.3.1 Effect of Residence Time on P Recovery

In contrast to the six-hour duration of the screening analysis, phosphorus recovery occurred significantly faster in the optimization experiments, as illustrated in Figure 5. This could be attributed to both the higher pH of the real wastewater (6.46 – 8.02 for the 100 MGD

https://doi.org/10.26434/chemrxiv-2024-gwpw5 **ORCID:** https://orcid.org/0000-0002-6737-415X Content not peer-reviewed by ChemRxiv. **License:** CC BY-NC-ND 4.0

plant) in comparison to the synthetic wastewater (6.25) and the use of the magnesium alloy as the anode. The pH level of the wastewater is an important factor for phosphorus recovery as it influences both the solubility of the precipitate and the solution supersaturation [65,66]. The high pH level in the real wastewater corresponds to a shorter time for the pH to increase to conditions where phosphorus recovery is most favorable, while the magnesium alloy also contributes to an accelerated overall pH increase in the system. These conditions are responsible for the increase in the bulk pH (8.28-9.10) of the wastewater after the electrochemical recovery experiment.

As shown in Figure 5, the average phosphorus recovery for all the runs was approximately 30 ± 11 % at 5 minutes, 45 ± 14 % at 10 minutes, 70 ± 14 % at 20 minutes, 87 ± 12 % at 30 minutes, 97 ± 3 % at 60 minutes, 98 ± 0.6 % at 90 minutes and 98.3 ± 0.3 % at 120 minutes. The variation within the data points, indicated by the standard deviation, significantly diminished after 30 minutes, signifying that beyond this time, varying the process conditions has minimal impact on phosphorus recovery efficiency. However, this does not negate the need for process condition optimization, as these variables also influence energy consumption and synthesis time, which must be optimized. Kékedy-Nagy *et al.* in their study on electrochemical nutrient removal using Mg anode and various natural wastewaters with initial pH levels ranging from 7.9 to 10.2, similarly reported phosphate removal efficiency between 44% and 93% within 30 minutes [23]. Therefore, this present study used 30 minutes as a threshold and developed a model at this time mark to describe the relationships between the factors and the system response, while also predicting the optimum conditions for maximum phosphorus recovery and minimum energy consumption.

https://doi.org/10.26434/chemrxiv-2024-gwpw5 **ORCID:** https://orcid.org/0000-0002-6737-415X Content not peer-reviewed by ChemRxiv. **License:** CC BY-NC-ND 4.0

Figure 5: Heatmap of P recovery under different process condition, illustrating the effect of residence time on electrochemical phosphorus recovery. Notably, after a residence time of 30 minutes, P recovery approaches 100% across all tested conditions, indicating that beyond this threshold, the effect of the process variables becomes negligible, as the recovery efficiency nears its maximum potential.

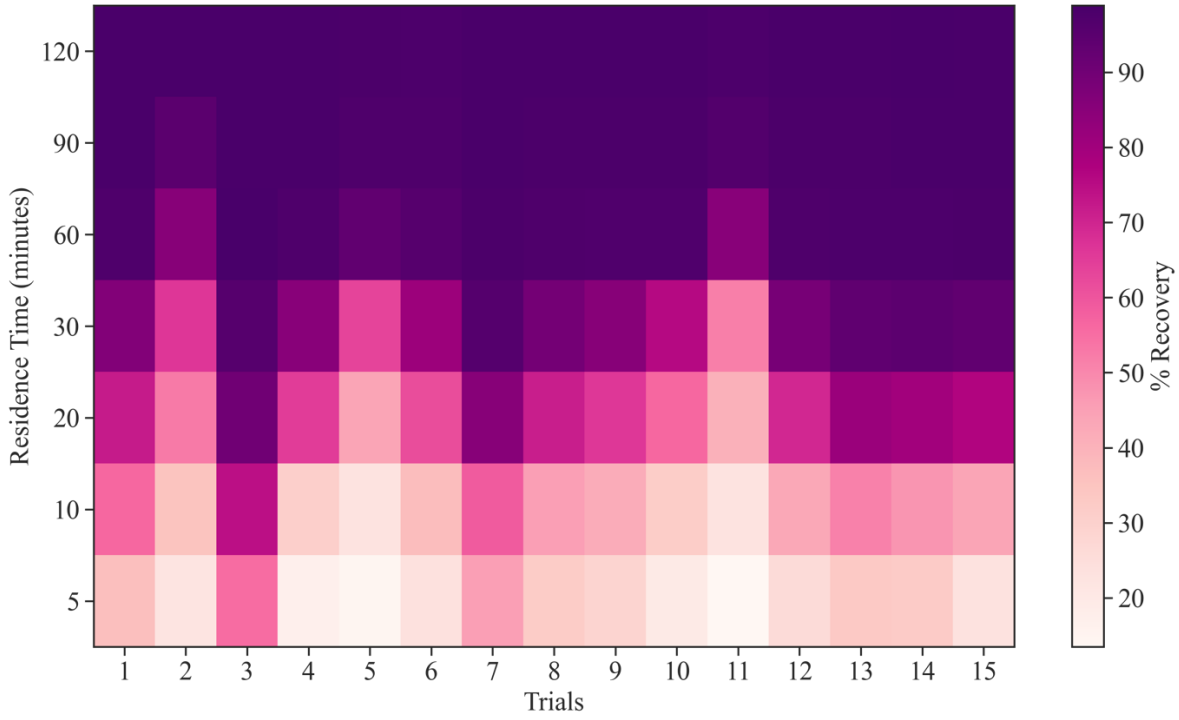

3.3.2 Response Surface Analyses and Model Validation

The regression models presented in the screening phase serves the purpose of eliminating less significant variables but does not capture the response's curvature, i.e., any non-linearity in the responses since there are only two points per variable. In this section, three distinct second-order models were constructed to characterize P recovery and E_s outcomes from the optimization experiments at the 30-minute time mark. These models included linear and square terms (SM), linear and interaction terms (IM), and full quadratic terms (FM). The regression equations and their associated R-squared values for P recovery and E_s responses are detailed in Table S13 and

https://doi.org/10.26434/chemrxiv-2024-gwpw5 **ORCID:** https://orcid.org/0000-0002-6737-415X Content not peer-reviewed by ChemRxiv. **License:** CC BY-NC-ND 4.0

Table S14, respectively. Based on these tables, the order of decreasing R-squared value of the models are FM, SM and IM. It is important to note that, as real wastewater was used in this set of experiments, the composition of ions could not be controlled in different experiments [67] and therefore, the responses exhibited less reproducibility, resulting in a model with smaller R-squared values (0.55 - 0.80) compared to the screening analysis model (0.97-0.99). The Pareto charts illustrating standardized effects for the two responses of the optimization experiments (Figures S7 and S9), the normal probability plots (Figures S8 and S10) as well as the statistical output (Tables S16 to S21) are provided in the supporting information.

These models combined with Minitab's response optimizer predicted 3 distinct conditions for maximum P % recovery – one for each model – and 2 distinct conditions for minimum energy consumption – FM and IM predicted the same set of conditions. These predicted optimization plots are illustrated in Figure S5 and Figure S6, while the optimum conditions for each model and both responses are provided in Table S15. The five sets of conditions were scaled down to two for model validation (Table 3): one set of conditions that were predicted to optimize both system responses and another set with values that were most different from this condition. Both conditions chosen were for maximum P % recovery, with the rationale that a global maximum for P recovery coupled with a local minimum for energy consumption, would be preferable to finding a global minimum for energy consumption and a local maximum for P % recovery. These conditions will be referred to as the Square Model Optimum Condition (SMOC) and the Interaction Model Optimum Condition (IMOC), based on the models that were used to predict these conditions.

https://doi.org/10.26434/chemrxiv-2024-gwpw5 **ORCID:** https://orcid.org/0000-0002-6737-415X Content not peer-reviewed by ChemRxiv. **License:** CC BY-NC-ND 4.0

Table 3. Conditions chosen for model validation based on the predicted values for the Square Model Optimum Condition (SMOC) and the Interaction Model Optimum Condition (IMOC) for maximum P recovery at 30 minutes

Factor	Cathodic Potential (V vs Ag/AgCl)	Area-Volume ratio (1/cm)	Temperature (°C)
SMOC	-1.29	0.129	41.3
IMOC	-0.805	0.146	41.3

The experimental P recoveries and their corresponding specific energies obtained at the SMOC and IMOC were 91.88% (0.96 kWh/kg P) and 94.60% (0.03 kWh/kg P), respectively. Figure 6 shows the models contour plots for phosphorus recovery and specific energy consumption, integrated with the experimentally obtained values. Although, the P recovery models (Figure 6a and b) predicted values greater than 100% at the optimum conditions, the experimental values are within the realistic range on the contour plots. Overall, the IMOC outperforms the SMOC with a higher P recovery and significantly lower specific energy consumption.

https://doi.org/10.26434/chemrxiv-2024-gwpw5 **ORCID:** https://orcid.org/0000-0002-6737-415X Content not peer-reviewed by ChemRxiv. **License:** CC BY-NC-ND 4.0

Figure 6: Contour plots of phosphorus recovery and specific energy consumption 41.3°C and as a function of cathodic potential and area-volume ratio based on (a) P Recovery Square model, (b) P Recovery Interaction model, (c) Specific Energy Square model and (d) Specific Energy Interaction model. The dark region in (a) and (b) denote areas where the models predict P recovery >100% while the white region in (c) and (d) represents regions where the model predicts specific energy consumption <0 kWh/kg. The square and circle markers represent the optimal values predicted by P Recovery Square and Interaction Models, respectively, while the values under the markers correspond to the experimental measurements at the predicted optimal conditions.

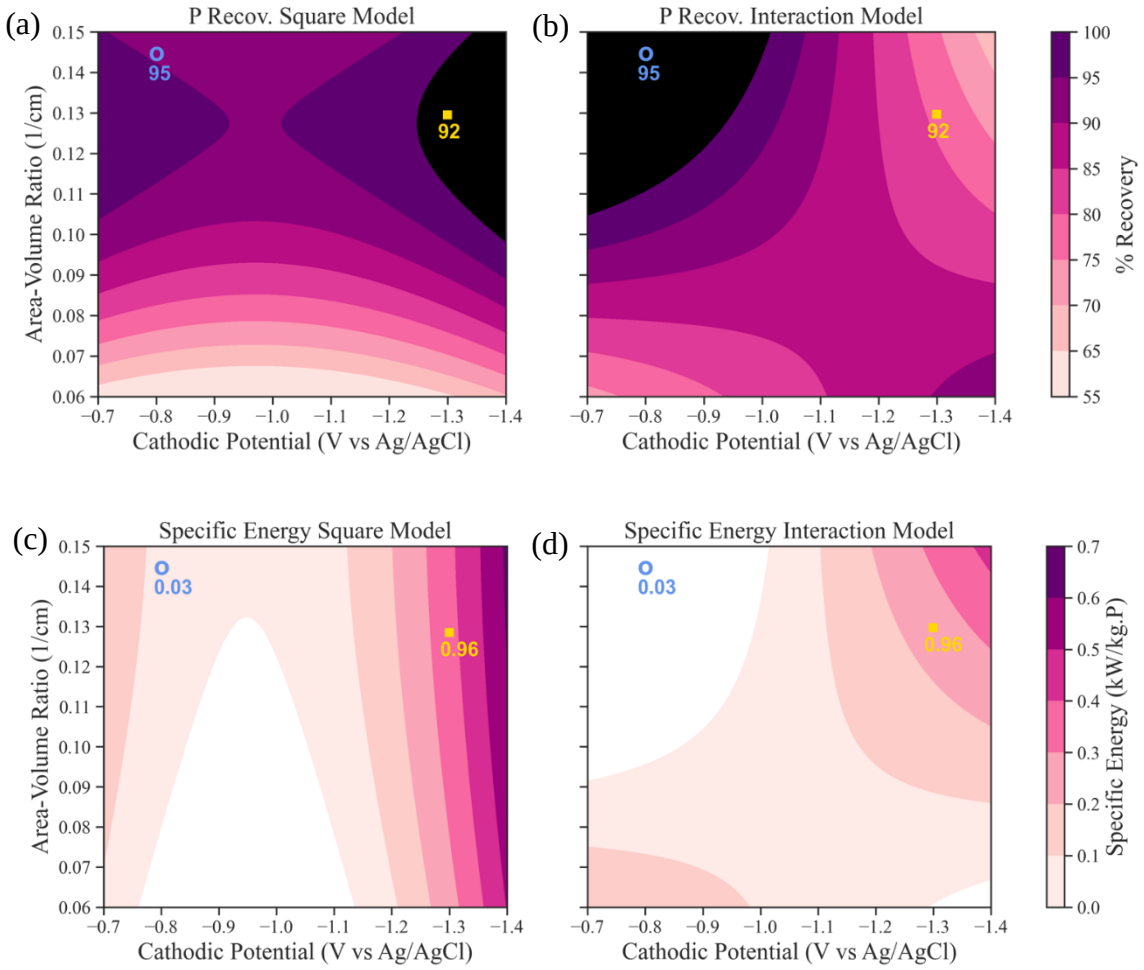

https://doi.org/10.26434/chemrxiv-2024-gwpw5 **ORCID:** https://orcid.org/0000-0002-6737-415X Content not peer-reviewed by ChemRxiv. **License:** CC BY-NC-ND 4.0

The Pareto charts in Figure S7 show that cathodic potential has the most significant effect on the specific energy consumption and is also predicted to have some effect on the P % recovery based on models that include interaction terms. Therefore, a cathodic potential of -1.29 V vs Ag/AgCl, predicted by the P recovery Square Model (SM), is expected to lead to high polarization of the electrodes, thus increasing the energy consumption. Although this should result in increased reaction kinetics and higher P recovery than the -0.805 V vs Ag/AgCl of Interaction Model (IM), the more negative potential also increases the rate of hydrogen generation, based on water reduction. This could reduce the surface area of the electrode available for phosphorus deposition if the H_2 bubbles are not quickly driven away by the impeller, thereby contributing to the slightly lower P recovery at the SMOC. Therefore, the optimum condition for high P recovery and low energy consumption, as predicted by the interaction model and confirmed experimentally, is at a less negative cathodic potential of -0.805 V vs Ag/AgCl, a high electrode area-volume ratio of 0.145 cm^{-1}, and a temperature of 41.3°C.

To evaluate the P recovery models' predictability and behavior of the variables, the SM was analyzed under both SMOC and IMOC, and a similar analysis was conducted for the IM, as depicted in Figure 6. The contour plot of the P recovery based on SM (Figure 6a) shows that the experimental P recovery at the SMOC (92%) falls below the SM predicted value (>100%), indicating an overprediction. Conversely, the experimentally obtained value at the IMOC (95%) closely aligns with the SM prediction at this condition (94%). Although the SM accurately predicts P recovery under the IMOC, this condition is in a region of the SM contour plot predicted to have a lower P recovery than SMOC. This suggests that the square model predicted optimum is not the true optimum region, challenging the response behavior of the variables as predicted by the model.

https://doi.org/10.26434/chemrxiv-2024-gwpw5 **ORCID:** https://orcid.org/0000-0002-6737-415X Content not peer-reviewed by ChemRxiv. **License:** CC BY-NC-ND 4.0

In contrast, the interaction model predictions overestimate P recovery (>100%) at the IMOC (95%) and underestimates it (80%) at the SMOC (92%) as shown in Figure 6b. Nonetheless, the IM's predicted optimum region aligns with experimental observation. Therefore, the IM proved more accurate for describing the relationship between the variables and P recovery. The IM indicates that at an area-volume ratio between 0.8 and 0.9, P recovery ranges between 85 and 90% and this recovery is consistent regardless of changes in the cathodic potential. However, outside this ratio, P recovery becomes more dependent on the cathodic potential. In the range of -0.7 to -1.1 V vs Ag/AgCl, P recovery increases with an increase in the area-volume ratio. Conversely, within the -1.2 to -1.4 V vs Ag/AgCl range, P recovery decreases as the area-volume ratio increases. These observations offer insights into the cathodic potential threshold for electrochemical phosphorus recovery. Particularly, these suggests that at potentials greater than -1.2 V vs Ag/AgCl, the increased generation of hydrogen gas, as previously discussed, could limit the solid-state growth of phosphate compounds.

The specific energies obtained experimentally under optimum phosphorus recovery conditions were compared with the E_s models in Figure 6c and d. Despite the E_s models' predictions being inaccurate, the substantial difference in energy values obtained experimentally at the SMOC (0.96 kWh/kg P) and IMOC (0.03 kWh/kg P) confirms the pronounced color contrast observed at these two points in the models. The specific energy consumed, as described in Equation 6, increases as cathodic potential becomes more negative and decreases as the amount of recovered phosphorus increases. Interestingly, at the P recovery IM in Figure 6b, the less negative cathodic potential and high area-volume ratio correlates with high phosphorus recovery. This correlation explains the apparent inverse relationship between the phosphorus recovery IM in Figure 6b and the specific energy IM in Figure 6d.

https://doi.org/10.26434/chemrxiv-2024-gwpw5 **ORCID:** https://orcid.org/0000-0002-6737-415X Content not peer-reviewed by ChemRxiv. **License:** CC BY-NC-ND 4.0

3.4 Phase Identification of the Recovered Products and Process Energy comparison

During the optimization experiments, precipitation occurred at the surfaces of the electrodes and in the bulk electrolyte. The recovered products showed multiple sharp peaks in the X-ray diffractograms in over 75% of the analyzed samples, which revealed that the recovered materials were predominantly crystalline. The remaining samples had little to no significant sharp diffraction peaks, an indicator of amorphous phase. Further examination of representative samples of the recovered crystalline products using SEM as depicted in Figure 7, showed these materials predominately consist of orthorhombic crystalline shapes, with a smaller portion having a thin platelet shape. The combination of different shapes is an indicator of a non-homogenous morphology in these samples. Finally, the EDS analyses indicated precipitates are primarily composed of Mg and P, with minimal Ca presence in both crystalline and amorphous groups of products.

The Rietveld refinement of the diffractograms of the mostly crystalline samples show struvite ICSD-60262 (ICSD web version 5.2.0) [68,69] as the major component with a volume fraction range of 87-91%. These samples also contained some amount of K-struvite ($MgKPO_4$•6 H_2O), ICSD30504 (ICSD web version 5.2.0) [69,70], with a range of 9-13%. The raw and refined XRD pattern of a representative sample is depicted in Figure 7c, with an R_w of 10.459 after refinement, consisting of 91% struvite and 9% K-struvite.

https://doi.org/10.26434/chemrxiv-2024-gwpw5 **ORCID:** https://orcid.org/0000-0002-6737-415X Content not peer-reviewed by ChemRxiv. **License:** CC BY-NC-ND 4.0

Figure 7: Recovered crystalline product phase identification showing SEM image and RGB mapping of a sample with a) smaller crystals and b) bigger crystals. Red represents Mg and green represents P, resulting in a yellow color in the area containing both elements. c) XRD pattern of a sample of the crystalline group in the 2θ range of 10-60 degrees (the full 10-90 range is shown in Figure S11) .

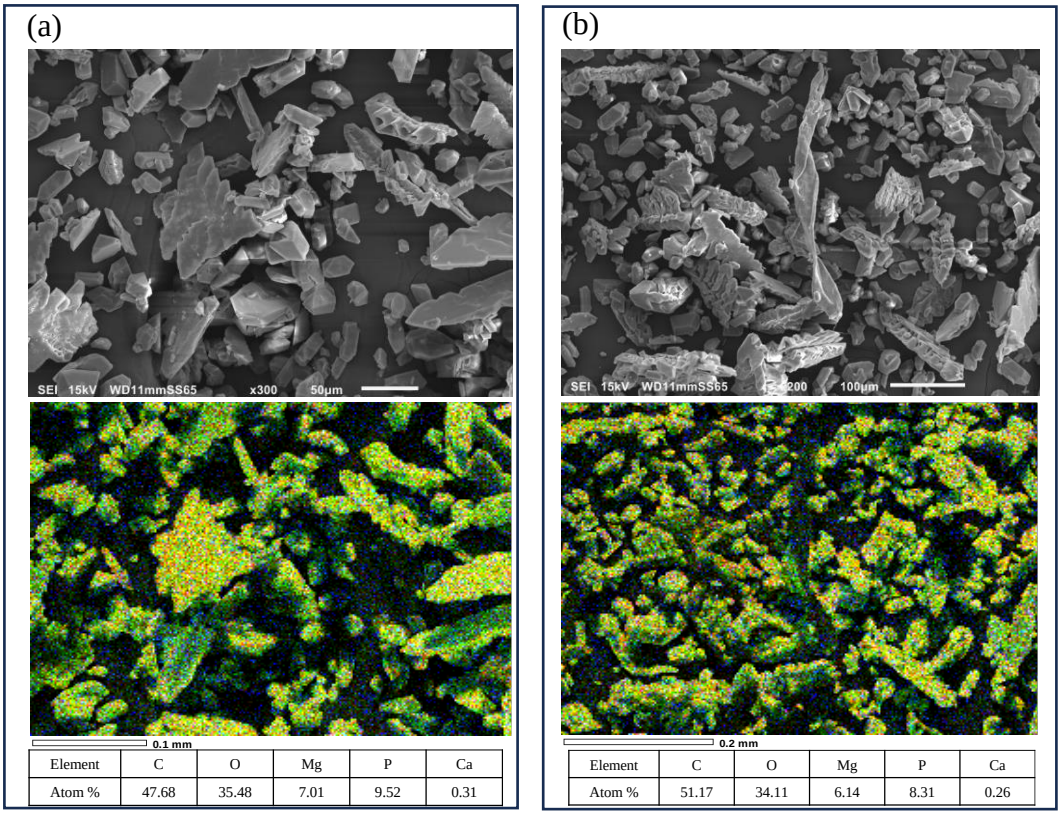

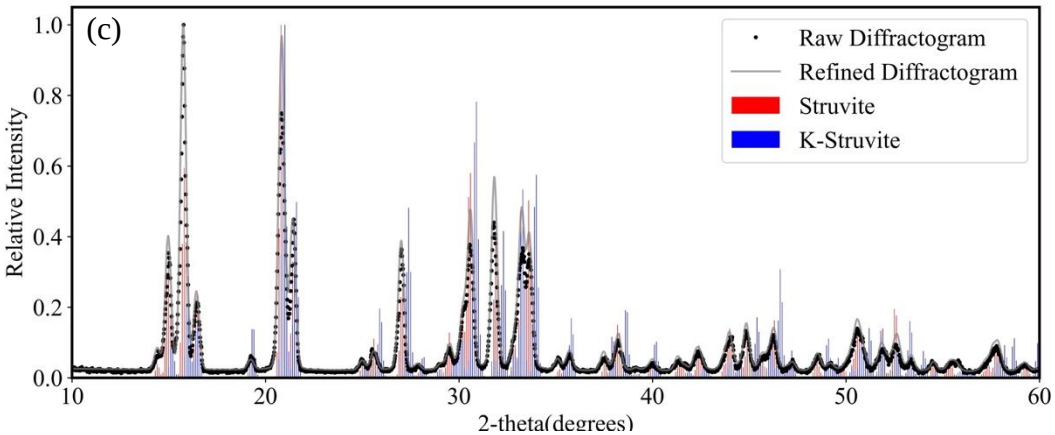

https://doi.org/10.26434/chemrxiv-2024-gwpw5 **ORCID:** https://orcid.org/0000-0002-6737-415X Content not peer-reviewed by ChemRxiv. **License:** CC BY-NC-ND 4.0

In addition, based on the SEM images represented in Figure 7a and b, while all these materials predominantly consisted of well-defined orthorhombic crystalline shapes, they had different sizes: there were small crystals with a length of 22 – 38 μm and larger crystals with lengths in the 82 – 131 μm range with a repetitive pattern in each agglomerate. Since struvite has a nucleation and growth type of formation [12], these length differences are probably due to the difference in the time the crystal has had to nucleate and grow.

Furthermore, the smaller amorphous fraction, which consist primarily of Mg and P as well, are likely an amorphous magnesium phosphate precipitate. However, since amorphous materials are a non-equilibrium category of compounds [71], the occurrence of an amorphous phase could be attributed to insufficient aging, i.e., before reaching equilibrium, for the crystalline phase. Ziegenheim *et al*. and Al-Hamzah *et al.* showed brucite was formed in an amorphous state when the experiment duration was short [72,73]. Additionally, literature has shown that while precipitating struvite or K-struvite ($MgKPO_4.6\ H_2O$) [74,75], an amorphous transition state occurred before the final crystallization step. Therefore, it is possible that the recovered products in the amorphous category of this study are also struvite, but precipitated quickly and require more than a 2-hour length-scale for crystallization . However, this hypothesis needs to be further tested via approaches that correlate precipitate size with crystalline or amorphous character and experimental conditions in a future work.

Lastly, the optimized electrochemical recovery process demonstrated a remarkably low energy consumption of 0.03 kWh/kg P, contrasting sharply with the global energy requirement for phosphorus fertilizer production in 2019, which stood at 1.15 kWh/kg P [76]. Additionally, the recovered phosphorus product in this study is predominantly struvite which creates opportunities

https://doi.org/10.26434/chemrxiv-2024-gwpw5 **ORCID:** https://orcid.org/0000-0002-6737-415X Content not peer-reviewed by ChemRxiv. **License:** CC BY-NC-ND 4.0

for further comparison with other electrochemical nutrient recovery processes that also utilize magnesium anodes to produce struvite. Hug and Udert reported energy consumption ranging from 0.1 to 2.2 kWh/kg P at 75% recovery, depending on the anodic potential [77]. Another study with synthetic wastewater reported a specific energy consumption value of 0.031 kWh/kg P at 500 mM Cl^-, which is not typical of municipal wastewater, and a range of 0.09 to 0.18 kWh/kg P for 5-50 mM Cl^-, a range more realistic for municipal wastewater [78]. These comparisons highlight the potential of the optimized electrochemical process in reducing the energy consumption of the aeration process in wastewater treatment plant through recovery of nutrients from the centrate stream, and also decreasing the national/global energy requirement for fertilizer production.

4 Conclusion

This comprehensive study investigated the characteristics of different municipal wastewater streams (aerobic, anaerobic dewatering and anaerobic thickening effluent) for nutrient recovery potential, screened out the unimportant operational, design and stream variables in electrochemical nutrient recovery and optimized these variables to maximize phosphorus recovery and minimize specific energy consumptions. The wastewater sampling showed a high calcium concentration in Athens aerobic, which, when coupled with its low ammonium concentration, suggests that phosphorus recovery via calcium phosphates, such as hydroxyapatite, is a more feasible route than struvite precipitation in this treatment plant. On the other hand, the low calcium concentration in Columbus anaerobic effluent indicated that the impact of calcium as a competing ion for phosphate recovery through struvite precipitation may be negligible, provided there is sufficient magnesium available for the reaction. Time series

https://doi.org/10.26434/chemrxiv-2024-gwpw5 **ORCID:** https://orcid.org/0000-0002-6737-415X Content not peer-reviewed by ChemRxiv. **License:** CC BY-NC-ND 4.0

analysis of the year-long sampling data revealed that major ions such as Ca^{2+} and Mg^{2+} exhibited interdependence with Ortho-P concentration. Additionally, the stream pH was found to correlate with Ortho-P and Cl^- in the anaerobic dewatering streams.

Screening analysis of electrochemical nutrient recovery identified anode type, cathodic potential, initial P concentration, initial NH_4 concentration and temperature to be the most important variables for phosphorus recovery and energy consumption, with either SS316 or SS304 as the cathode. However, the SS316 typically provided higher P recovery than SS304. In the optimization analysis, phosphorus recovery occurs significantly faster, due to the higher pH in the real wastewater. Consequently, phosphorus recovery peaks after 30 minutes of an experimental run; thus, minimizing the impact of the process variables. The optimum condition for high P recovery and low specific energy consumption from the anaerobic digester wastewater was a cathodic potential of -0.805 V vs Ag/AgCl, electrode area-volume ratio of 0.145 cm^{-1}, and a temperature of 41.3°C, as predicted by the interaction model and confirmed experimentally. Finally, solid characterization of the recovered products from the optimization analyses revealed a combination of struvite (87-91%) and K-struvite (9-13%), with traces of calcium deposits. Future work should investigate the potential for real-world pilot demonstrations at WWTPs supported by cost estimation of fertilizer production at different WWTP scales.

5 Acknowledgements

The authors acknowledge the assistance from and discussions with employees at both WWTPs during the sampling phase of this study, especially the plant managers including Darin Wise (former Southerly Plant Manager), Doug Dixon Junior (current Southerly Plant Manager) and Lisa Agriesti (City of Athens Plant Manager). We also acknowledge Dr. Babatunde I. Ojoawo for assistance with sampling logistics and Dr. Brian Lejeune for assistance with the

https://doi.org/10.26434/chemrxiv-2024-gwpw5 **ORCID:** https://orcid.org/0000-0002-6737-415X Content not peer-reviewed by ChemRxiv. **License:** CC BY-NC-ND 4.0

Rietveld refinement of the X-Ray Diffractograms. Furthermore, the authors acknowledge funding from the U.S. Department of Energy's Office of Energy Efficiency and Renewable Energy (EERE) under the Industrial Efficiency and Decarbonization Office, Research and Development for Advanced Water Resource Recovery Systems award number DE-EE0009502. This report was prepared as an account of work sponsored by an agency of the United States Government. Neither the United States Government nor any agency thereof, nor any of its employees, makes any warranty, express or implied, or assumes any legal liability or responsibility for the accuracy, completeness, or usefulness of any information, apparatus, product, or process disclosed, or represents that its use would not infringe privately owned rights. Reference herein to any specific commercial product, process, or service by trade name, trademark, manufacturer, or otherwise does not necessarily constitute or imply its endorsement, recommendation, or favoring by the United States Government or any agency thereof. The views and opinions of authors expressed herein do not necessarily state or reflect those of the United States Government or any agency thereof.

https://doi.org/10.26434/chemrxiv-2024-gwpw5 **ORCID:** https://orcid.org/0000-0002-6737-415X Content not peer-reviewed by ChemRxiv. **License:** CC BY-NC-ND 4.0

6 References

1. Copeland, C. & Carter, N. T. Energy-Water Nexus: The Water Sector's Energy Use. *Wash. DC Congr. Res. Serv.* (2017).
2. E Source. Wastewater Treatment Plants. *Business Energy Advisor* https://esource.bizenergyadvisor.com/article/wastewater-treatment-plants (2020).
3. Pabi, S., Amarnath, A. & Goldstein, R. Electricity Use and Management in the Municipal Water Supply and Wastewater Industries. *Water Res. Found.* (2013).
4. Crawford, G. V. & Sandino, J. *Energy Efficiency in Wastewater Treatment in North America: A Compendium of Best Practices and Case Studies of Novel Approaches: [Final Report]*. (Water Environment Research Foundation ; IWA Publishing, Alexandria, VA : London, United Kingdom, 2010).
5. The Engineering ToolBox. Solubility of Gases in Water vs. Temperature. https://www.engineeringtoolbox.com/gases-solubility-water-d_1148.html.
6. Devos, P., Filali, A., Grau, P. & Gillot, S. Sidestream characteristics in water resource recovery facilities: A critical review. *Water Res.* **232**, 119620 (2023).
7. Balaguer-Barbosa, M. Recovery of Nutrients from Anaerobically Digested Enhanced Biological Phosphorus Removal (EBPR) Sludge through Struvite Precipitation. *USF Tampa Grad. Theses Diss.* (2018).
8. Campos, J. L. *et al.* Nitrogen and Phosphorus Recovery From Anaerobically Pretreated Agro-Food Wastes: A Review. *Front. Sustain. Food Syst.* **2**, (2019).
9. Wang, C.-C., Hao, X.-D., Guo, G.-S. & van Loosdrecht, M. C. M. Formation of pure struvite at neutral pH by electrochemical deposition. *Chem. Eng. J.* **159**, 280–283 (2010).

https://doi.org/10.26434/chemrxiv-2024-gwpw5 **ORCID:** https://orcid.org/0000-0002-6737-415X Content not peer-reviewed by ChemRxiv. **License:** CC BY-NC-ND 4.0

10. de-Bashan, L. E. & Bashan, Y. Recent advances in removing phosphorus from wastewater and its future use as fertilizer (1997-2003). *Water Res.* **38**, 4222–4246 (2004).
11. Guštin, S. & Marinšek-Logar, R. Effect of pH, temperature and air flow rate on the continuous ammonia stripping of the anaerobic digestion effluent. *Process Saf. Environ. Prot.* **89**, 61–66 (2011).
12. Le Corre, K. S., Valsami-Jones, E., Hobbs, P. & Parsons, S. A. Phosphorus Recovery from Wastewater by Struvite Crystallization: A Review. *Crit. Rev. Environ. Sci. Technol.* **39**, 433–477 (2009).
13. Krishnamoorthy, N. *et al*. Engineering principles and process designs for phosphorus recovery as struvite: A comprehensive review. *J. Environ. Chem. Eng.* **9**, 105579 (2021).
14. Münch, E. V. & Barr, K. Controlled struvite crystallisation for removing phosphorus from anaerobic digester sidestreams. *Water Res.* **35**, 151–159 (2001).
15. Ansari, A. J., Hai, F. I., Price, W. E., Drewes, J. E. & Nghiem, L. D. Forward osmosis as a platform for resource recovery from municipal wastewater - A critical assessment of the literature. *J. Membr. Sci.* **529**, 195–206 (2017).
16. Parsons, S. A. & Smith, J. A. Phosphorus Removal and Recovery from Municipal Wastewaters. *Elements* **4**, 109–112 (2008).
17. Malamis, S., Katsou, E., Di Fabio, S., Bolzonella, D. & Fatone, F. Biological nutrients removal from the supernatant originating from the anaerobic digestion of the organic fraction of municipal solid waste. *Crit. Rev. Biotechnol.* **34**, 244–257 (2014).
18. Wei, Y., Van Houten, R. T., Borger, A. R., Eikelboom, D. H. & Fan, Y. Minimization of excess sludge production for biological wastewater treatment. *Water Res.* **37**, 4453–4467 (2003).

https://doi.org/10.26434/chemrxiv-2024-gwpw5 **ORCID:** https://orcid.org/0000-0002-6737-415X Content not peer-reviewed by ChemRxiv. **License:** CC BY-NC-ND 4.0

19. Bagastyo, A. Y. *et al.* Electrochemically-driven struvite recovery: Prospect and challenges for the application of magnesium sacrificial anode. *Sep. Purif. Technol.* **288**, 120653 (2022).
20. Belarbi, Z., Daramola, D. A. & Trembly, J. P. Bench-Scale Demonstration and Thermodynamic Simulations of Electrochemical Nutrient Reduction in Wastewater via Recovery as Struvite. *J. Electrochem. Soc.* **167**, 155524 (2020).
21. Ye, Y. *et al.* Insight into chemical phosphate recovery from municipal wastewater. *Sci. Total Environ.* **576**, 159–171 (2017).
22. Ghosh, S., Lobanov, S. & Lo, V. K. An overview of technologies to recover phosphorus as struvite from wastewater: advantages and shortcomings. *Environ. Sci. Pollut. Res.* **26**, 19063–19077 (2019).
23. Kékedy-Nagy, L. *et al.* Electrochemical nutrient removal from natural wastewater sources and its impact on water quality. *Water Res.* **210**, 118001 (2022).
24. Ojoawo, B. I. & Daramola, D. A. Multivariate screening analyses of electrochemically driven nutrient recovery from wastewater using nutrient removal and energy consumption as responses. *Resour. Conserv. Recycl. Adv.* **20**, 200194 (2023).
25. Lei, Y., Zhan, Z., Saakes, M., van der Weijden, R. D. & Buisman, C. J. N. Electrochemical Recovery of Phosphorus from Acidic Cheese Wastewater: Feasibility, Quality of Products, and Comparison with Chemical Precipitation. *ACS EST Water* **1**, 1002–1013 (2021).
26. Dickey, D. A. & Fuller, W. A. Distribution of the Estimators for Autoregressive Time Series with a Unit Root. *J. Am. Stat. Assoc.* **74**, 427–431 (1979).
27. Brockwell, P. J. & Davis, R. A. *Introduction to Time Series and Forecasting*. (Springer International Publishing, Cham, 2016). doi:10.1007/978-3-319-29854-2.

https://doi.org/10.26434/chemrxiv-2024-gwpw5 **ORCID:** https://orcid.org/0000-0002-6737-415X Content not peer-reviewed by ChemRxiv. **License:** CC BY-NC-ND 4.0

28. National Institute of Standards and Technology (NIST). 5.3.3.5. Plackett-Burman designs. https://www.itl.nist.gov/div898/handbook/pri/section3/pri335.htm.
29. Montgomery, D. C., Runger, G. C. & Hubele, N. F. *Engineering Statistics*. (John Wiley, Hoboken, NJ, 2011).
30. Minitab. Coefficients table for Analyze Definitive Screening Design. https://support.minitab.com/en-us/minitab/help-and-how-to/statistical-modeling/doe/how-to/screening/analyze-screening-design/interpret-the-results/all-statistics-and-graphs/coefficients-table/.
31. Minitab. Interpret the key results for Analyze Definitive Screening Design. https://support.minitab.com/en-us/minitab/help-and-how-to/statistical-modeling/doe/how-to/screening/analyze-screening-design/interpret-the-results/key-results/.
32. Minitab. Effects plots for Analyze Definitive Screening Design. https://support.minitab.com/en-us/minitab/help-and-how-to/statistical-modeling/doe/how-to/screening/analyze-screening-design/interpret-the-results/all-statistics-and-graphs/effects-plots/.
33. Minitab. Residual plots for Analyze Definitive Screening Design. https://support.minitab.com/en-us/minitab/help-and-how-to/statistical-modeling/doe/how-to/screening/analyze-screening-design/interpret-the-results/all-statistics-and-graphs/residual-plots/.
34. Seaborn: statistical data visualization. Seaborn.kdeplot — seaborn 0.13.2 documentation. https://seaborn.pydata.org/generated/seaborn.kdeplot.html.
35. Thompson, M. & Walsh, J. N. *Handbook of Inductively Coupled Plasma Spectrometry*. (Springer US, Boston, MA, 1989). doi:10.1007/978-1-4613-0697-9.

https://doi.org/10.26434/chemrxiv-2024-gwpw5 **ORCID:** https://orcid.org/0000-0002-6737-415X Content not peer-reviewed by ChemRxiv. **License:** CC BY-NC-ND 4.0

36. Schneider, C. A., Rasband, W. S. & Eliceiri, K. W. NIH Image to ImageJ: 25 years of image analysis. *Nat. Methods* **9**, 671–675 (2012).

37. Toby, B. H. & Von Dreele, R. B. GSAS-II: the genesis of a modern open-source all purpose crystallography software package. *J. Appl. Crystallogr.* **46**, 544–549 (2013).

38. Rietveld, H. M. A profile refinement method for nuclear and magnetic structures. *J. Appl. Crystallogr.* **2**, 65–71 (1969).

39. Larson, A. C. & Dreele, R. B. V. GENERAL STRUCTURE ANALYSIS SYSTEM (GSAS). *Los Alamos Natl. Lab. Rep. LAUR 86-748* (2004).

40. Wolfe, K. D., Zanganeh, A., Arthur, R. N., Trembly, J. P. & Daramola, D. A. Considerations for Electrochemical Phosphorus Precipitation: A Figures of Merit Approach. *Electrochem. Soc. Interface* **32**, 51 (2023).

41. Metcalf & Eddy, Inc., Tchobanoglous, G., Stensel, H. D., Tsuchihashi, R. & Burton, F. *Wastewater Engineering: Treatment and Resource Recovery*. (McGraw-Hill Education, New York, 2014).

42. Hallas, J. F., Mackowiak, C. L., Wilkie, A. C. & Harris, W. G. Struvite Phosphorus Recovery from Aerobically Digested Municipal Wastewater. *Sustainability* **11**, 376 (2019).

43. Integrated co-limitation kinetic model for microalgae growth in anaerobically digested municipal sludge centrate. *Algal Res.* **18**, 15–24 (2016).

44. Wang, L. *et al.* Cultivation of Green Algae Chlorella sp. in Different Wastewaters from Municipal Wastewater Treatment Plant. *Appl. Biochem. Biotechnol.* **162**, 1174–1186 (2010).

45. *Water Reuse: Potential for Expanding the Nation's Water Supply Through Reuse of Municipal Wastewater*. (National Academies Press, Washington, D.C., 2012). doi:10.17226/13303.

https://doi.org/10.26434/chemrxiv-2024-gwpw5 **ORCID:** https://orcid.org/0000-0002-6737-415X Content not peer-reviewed by ChemRxiv. **License:** CC BY-NC-ND 4.0

46. Hach Company. Ammonia and Ammonium. https://www.hach.com/parameters/ammonia.
47. Drexler, I. L. C., Prieto, A. L. & Yeh, D. Wastewater Constituents. in *Comprehensive Water Quality and Purification* 7–29 (Elsevier, 2014). doi:10.1016/B978-0-12-382182-9.00043-8.
48. City of Athens. *Annual Drinking Water Consumer Confidence Report*. https://www.athensapr.com/DocumentCenter/View/8903/2020-Consumer-Confidence-Report?bidId= (2020).
49. The City of Columbus. Current Consumer Confidence Report. https://www.columbus.gov/Services/Public-Utilities/Information-for-Customers/Current-Consumer-Confidence-Report.
50. Pindine, G. P., Trembly, J. P. & Daramola, D. A. Equilibrium-Based Temperature-Dependent Economic Analysis of the Recovery of Phosphorus from Different Wastewater Streams via Chemical Precipitation. *ACS EST Water* **1**, 2318–2326 (2021).
51. Chen, R.-F., Liu, T., Rong, H.-W., Zhong, H.-T. & Wei, C.-H. Effect of Organic Substances on Nutrients Recovery by Struvite Electrochemical Precipitation from Synthetic Anaerobically Treated Swine Wastewater. *Membranes* **11**, 594 (2021).
52. United States Department of Agriculture. *Heavy Metal Soil Contamination*. https://semspub.epa.gov/work/03/2227185.pdf (2000).
53. Daneshgar, S., Buttafava, A., Capsoni, D., Callegari, A. & Capodaglio, A. G. Impact of pH and Ionic Molar Ratios on Phosphorous Forms Precipitation and Recovery from Different Wastewater Sludges. *Resources* **7**, 71 (2018).
54. Capdevielle, A., Sýkorová, E., Biscans, B., Béline, F. & Daumer, M.-L. Optimization of struvite precipitation in synthetic biologically treated swine wastewater--determination of the optimal process parameters. *J. Hazard. Mater.* **244–245**, 357–369 (2013).

https://doi.org/10.26434/chemrxiv-2024-gwpw5 **ORCID:** https://orcid.org/0000-0002-6737-415X Content not peer-reviewed by ChemRxiv. **License:** CC BY-NC-ND 4.0

55. Liu, X., Zhong, H., Yang, Y., Yuan, L. & Liu, S. Phosphorus removal from wastewater by waste concrete: influence of P concentration and temperature on the product. *Environ. Sci. Pollut. Res.* **27**, 10766–10777 (2020).

56. Belarbi, Z. & Trembly, J. P. Electrochemical Processing to Capture Phosphorus from Simulated Concentrated Animal Feeding Operations Waste. *J. Electrochem. Soc.* **165**, E685 (2018).

57. Ronteltap, M., Maurer, M., Hausherr, R. & Gujer, W. Struvite precipitation from urine – Influencing factors on particle size. *Water Res.* **44**, 2038–2046 (2010).

58. Wang, Y. *et al.* Electrochemically mediated precipitation of phosphate minerals for phosphorus removal and recovery: Progress and perspective. *Water Res.* **209**, 117891 (2022).

59. Tsang, D. C. W. Chapter 2 - Influence of Natural Organic Matter on Contaminant Removal by Permeable Reactive Barrier. in *The Role of Colloidal Systems in Environmental Protection* (ed. Fanun, M.) 19–40 (Elsevier, Amsterdam, 2014). doi:10.1016/B978-0-444-63283-8.00002-8.

60. Lei, Y., Song, B., Saakes, M., van der Weijden, R. D. & Buisman, C. J. N. Interaction of calcium, phosphorus and natural organic matter in electrochemical recovery of phosphate. *Water Res.* **142**, 10–17 (2018).

61. Wang, Y., Xiao, Q., Zhong, H., Zheng, X. & Wei, Y. Effect of organic matter on phosphorus recovery from sewage sludge subjected to microwave hybrid pretreatment. *J. Environ. Sci.* **39**, 29–36 (2016).

62. Feliu, S., Veleva, L. & García-Galvan, F. Effect of Temperature on the Corrosion Behavior of Biodegradable AZ31B Magnesium Alloy in Ringer's Physiological Solution. *Metals* **9**, 591 (2019).

https://doi.org/10.26434/chemrxiv-2024-gwpw5 **ORCID:** https://orcid.org/0000-0002-6737-415X Content not peer-reviewed by ChemRxiv. **License:** CC BY-NC-ND 4.0

63. Rossrucker, L., Mayrhofer, K. J. J., Frankel, G. S. & Birbilis, N. Investigating the Real Time Dissolution of Mg Using Online Analysis by ICP-MS. *J. Electrochem. Soc.* **161**, C115 (2014).

64. Kocijan, A., Donik, Č. & Jenko, M. Electrochemical and XPS studies of the passive film formed on stainless steels in borate buffer and chloride solutions. *Corros. Sci.* **49**, 2083–2098 (2007).

65. Peng, L., Dai, H., Wu, Y., Peng, Y. & Lu, X. A comprehensive review of phosphorus recovery from wastewater by crystallization processes. *Chemosphere* **197**, 768–781 (2018).

66. Graziani, M. & McLean, D. Phosphorus Treatment and Removal Technologies. *Minn. Pollut. Control Agency* (2006).

67. O'Flaherty, E. & Gray, N. F. A comparative analysis of the characteristics of a range of real and synthetic wastewaters. *Environ. Sci. Pollut. Res.* **20**, 8813–8830 (2013).

68. Ferraris, G., H., F. & W., J. Neutron diffraction study of MgNH4PO4.6H2O (struvite) and survey of water molecules donating short hydrogen bonds. *Acta Crystallogr. B* **b42**, 253–258 (1986).

69. Zagorac, D., Müller, H., Ruehl, S., Zagorac, J. & Rehme, S. Recent developments in the Inorganic Crystal Structure Database: theoretical crystal structure data and related features. *J. Appl. Crystallogr.* **52**, 918–925 (2019).

70. Mathew, M. & Schroeder, L. W. Crystal structure of a struvite analogue, MgKPO4.6H2O. *Acta Crystallogr. Sect. B* **35**, 11–13 (1979).

71. Hu, Z.-Q., Wang, A.-M. & Zhang, H.-F. Chapter 22 - Amorphous Materials. in *Modern Inorganic Synthetic Chemistry (Second Edition)* (eds. Xu, R. & Xu, Y.) 641–667 (Elsevier, Amsterdam, 2017). doi:10.1016/B978-0-444-63591-4.00022-7.

https://doi.org/10.26434/chemrxiv-2024-gwpw5 **ORCID:** https://orcid.org/0000-0002-6737-415X Content not peer-reviewed by ChemRxiv. **License:** CC BY-NC-ND 4.0

72. Ziegenheim, S. *et al.* Differential Precipitation of Mg(OH)2 from CaSO4·2H2O Using Citrate as Inhibitor—A Promising Concept for Reagent Recovery from MgSO4 Waste Streams. *Molecules* **25**, 5012 (2020).
73. Al-Hamzah, A. A., Smith, E. J. & Fellows, C. M. Inhibition of Homogeneous Formation of Magnesium Hydroxide by Low-Molar-Mass Poly(acrylic acid) with Different End-Groups. *Ind. Eng. Chem. Res.* **54**, 2201–2207 (2015).
74. Gardner, L. J. *et al.* Characterization of and Structural Insight into Struvite-K, MgKPO4·6H2O, an Analogue of Struvite. *Inorg. Chem.* **60**, 195–205 (2021).
75. Hövelmann, J. *et al.* Struvite Crystallisation and the Effect of Co2+ Ions. *Minerals* **9**, 503 (2019).
76. Daramola, D. A. & Hatzell, M. C. Energy Demand of Nitrogen and Phosphorus Based Fertilizers and Approaches to Circularity. *ACS Energy Lett.* **8**, 1493–1501 (2023).
77. Hug, A. & Udert, K. M. Struvite precipitation from urine with electrochemical magnesium dosage. *Water Res.* **47**, 289–299 (2013).
78. Sultana, R., Kékedy-Nagy, L., Daneshpour, R. & Greenlee, L. F. Electrochemical recovery of phosphate from synthetic wastewater with enhanced salinity. *Electrochimica Acta* **426**, 140848 (2022).

https://doi.org/10.26434/chemrxiv-2024-gwpw5 **ORCID:** https://orcid.org/0000-0002-6737-415X Content not peer-reviewed by ChemRxiv. **License:** CC BY-NC-ND 4.0